EUROFUSION WP14ER-PR(15) 14051

F. Deluzet et al.

Asymptotic-preserving Particle-In-Cell methods for the Vlasov-Maxwell system near quasi-neutrality

Preprint of Paper to be submitted for publication in
Journal of Computational Physics

This work has been carried out within the framework of the EUROfusion Consortium and has received funding from the Euratom research and training programme 2014-2018 under grant agreement No 633053. The views and opinions expressed herein do not necessarily reflect those of the European Commission.

Asymptotic-preserving Particle-In-Cell methods for the Vlasov-Maxwell system near quasi-neutrality

P. Degond[†], F. Deluzet[‡], D. Doyen[⋆]

[†]Department of Mathematics, Imperial College London,
London SW7 2AZ, United Kingdom,
pdegond@imperial.ac.uk

[‡]Université de Toulouse; UPS, INSA, UT1, UTM, Institut de Mathématiques de Toulouse,
CNRS, Institut de Mathematiques de Toulouse UMR 5219, F-31062 Toulouse, France,
fabrice.deluzet@math.univ-toulouse.fr

[⋆]Université de Marne-la-Vallée, Laboratoire d'Analyse et de Mathématiques Appliquées,
CNRS, Laboratoire d'Analyse et de Mathématiques Appliquées UMR 8050,
5, boulevard Descartes, Cité Descartes - Champs-sur-Marne, F-77454 Marne-la-Valle, France,
david.doyen@univ-mlv.fr

May 29, 2015

Abstract

This paper is devoted to the design of a numerical method for the efficient simulation of kinetic description of magnetized plasmas that may depart from the quasi-neutral regime. Precisely, the goal is to introduce a method offering a quasi-neutral description of the plasma when its evolution is governed by macroscopic scales but returns to more refined modelling when this assumption is broken. Quasi-neutral description of plasmas ease the derivation of efficient numerical methods because the fastest frequencies as well as the smallest space scales are filtered out from the equations. However the range of validity of these models is limited. The purpose is thus to derive numerical methods which conciliate the advantages of both descriptions. To address this question, the formalism of Asymptotic-Preserving methods is implemented in the framework of the Vlasov-Maxwell system in the quasi-neutral limit. The key step consists of the reformulation of this system which unifies the two regimes in a single set of equations with a smooth transition from one to another. This systematic derivation is detailed on the continuous set of equations and then brought to the Particle-In-Cell formalism.

1 Introduction

In a plasma, the Coulomb interaction between charged particles tends to restore the charge neutrality, while the thermal motion tends to disturb it. These opposing phenomena introduce a typical length of the separation between the electronic (n_e) and the ionic (n_i) densities, called the Debye length, and a typical oscillation period of the electrons, the plasma period. These plasma parameters depend essentially on the density and the temperature of the particles. In many applications, these scales are small compared to the global plasma evolution, therefore the plasma can be considered as a good electrical conductor so that the electric field E can be determined by macroscopic spatial and temporal scales [24, 38]. In that case, the Poisson's (Maxwell-Gauss) equation is meaningless for the computation of the electrostatic field because the

macroscopic quantities vary on much larger scales than the plasma parameters. This is the so-called *plasma approximation* translating that "*In a plasma it is possible to assume* $n_i = n_e$ *and* $\nabla \cdot E \neq 0$ *at the same time*" leading to the following conclusion "*Do not use Poisson's equation to obtain* E *unless it is unaviodable !*" [11, chapter 3]. This is precisely the aim of this paper: deriving a numerical method implementing a quasi-neutral description of the plasma in regions where its evolution is driven by macroscopic space and time scales, but with a non quasi-neutral description where this approximation is not sufficient. Note, that, for magnetized plasmas, the conclusion stated above concerning the use of the Maxwell-Gauss equation also applies for the Maxwell-Ampere equation.

In many plasma problems, some areas may be considered quasi-neutral, while some others are far from this regime, the interfaces between these regions may evolve with time, the density of the plasma, its temperature or the scales of interest being not necessarily uniform and time independent. That is the case, for instance, with problems involving plasma-vacuum interfaces, interactions of an electromagnetic wave with a dense plasma, or with the formation of non quasi-neutral sheaths. The idea of using a quasi-neutral description for the plasma is widely adopted, since it allows to filter out the fastest time scales and the smallest space scales from the equations, namely the plasma frequency and the Debye length. Numerical methods implementing these plasma descriptions are free from these severe restrictions on the discretization parameters, the most convincing example being the success of Magneto-Hydro-Dynamic numerical models for fluid description of plasmas or for instance [30, 34, 1] for quasi-neutral kinetic models. As mentioned above, this class of modeling, though offering efficient numerical tools for the plasma evolution on large scales, is not appropriate to describe all the complex physics that may occur in non quasi-neutral regions which are critical for the overall evolution of the system.

From a mathematical viewpoint, the plasma models (fluid or kinetic) change of nature in the quasi-neutral limit. The Maxwell-Ampere as well as the Maxwell-Gauss equations are degenerated under the quasi-neutral assumption, calling for alternative means of computing the electrostatic field in the limit regime. This kind of asymptotic is referred to as a singular limit. Therefore, the numerical solution of such problems requires either a coupling strategy (two different discretizations, one for the quasi-neutral area, one for the rest of the domain, coupled through an interface or by other means, this topic being subject of an active research) or a so-called Asymptotic-Preserving discretization. Such an Asymptotic-Preserving discretization satisfies the following three properties.

P1. For fixed Debye length and plasma period, the discretization is consistent with the standard plasma model when the discretization parameters tend to zero.

P2. The stability condition does not depend on either the Debye length or the plasma period (this later requirement will be clarified by the scaling relations).

P3. For fixed discretization parameters, the discretization is consistent with the quasi-neutral model when the Debye length and the plasma period tend to zero.

The concept of Asymptotic-Preserving method is not restricted to quasi-neutral plasma problems. Introduced by S. Jin [33] for transport in diffusive regimes, it has been applied to various singular limit problems: hydrodynamic or diffusion limit of kinetic models, relaxation limit of hyperbolic model, relaxation limit of complex Ginzburg-Landau equations, low-Mach number limit of compressible fluid model, limit of plasma model under large magnetic field, etc... Some references for these works can be found in [19]. In the case of plasmas near quasi-neutrality, Asymptotic-Preserving discretizations have already been developed for the Euler-Poisson [17], Euler-Maxwell [21] and Vlasov-Poisson models [5, 20]. The purpose of the present paper is to carry on the work initiated in these former realizations and derive Asymptotic-Preserving Particle-In-Cell methods for the Vlasov-Maxwell system in the quasi-neutral regime.

The key idea for the design of an Asymptotic-Preserving method lies in the reformulation of the original problem in a set of equivalent equations in which the asymptotic limit is a regular perturbation. Following the general methodology described in [19], this reformulated system is constructed in order to unify the two regimes, with a smooth transition from one to another accordingly to the asymptotic parameter value, preventing thus the degeneracy of the equations in the asymptotic limit. The reformulated system meets

thus the condition P3. Generally speaking, Asymptotic-Preserving schemes are implicit time discretizations, which ensures also that the condition P2 is met.

Another important issue is related to the Particle-In-Cell method selected for the discretization of the Vlasov-Maxwell system. Standard PIC methods are well documented (see for instance [3, 36, 4]) to lack consistency with the continuity equation, translating the total conservation of the charge. Different cures to this flaw can be envisioned, the most popular being an elliptic correction of the electric field. This process is extended to the Asymptotic-Preserving framework in order to derive an efficient and meaningful numerical method.

The organization of the paper is the following. The section 2 is devoted to the statement of the Vlasov-Maxwell system and more precisely to the Generalysed Vlasov-Maxwell system incorporating the electric field correction. The assumptions of the quasi-neutral regime are then precised. The asymptotics investigated in this work borrows most of the assumptions of the Magneto-Hydro-Dynamic models, but with a kinetic description for both the electrons and the ions and a finite inertia for electrons. A dimensionless parameter is introduced, namely the scaled Debye length, to identify the transition between the two regimes. The singular nature of the quasi-neutral limit is clearly identified and explained by the vanishing, in the Maxwell-Ampere and Maxwell-Gauss equations, of the terms carrying the electric field. This quantity can however be determined in the quasi-neutral regime thanks to macroscopic equations, so that a limit model (providing a means of computing all the unknowns) can be stated. The reformulation of the system is thus addressed with the aim to manufacture a set of equations, equivalent to the Generalysed Vlasov-Maxwell system but, in which, the quasi-neutral limit is regular: the limit model is recovered from this reformulated system by setting the asymptotic parameter to zero. The discretization is detailed in the section 3. The Particle-In-Cell method main concepts are recalled with the definition of a standard scheme used as a reference for the AP-methods. The Asymptotic-Preserving time discretization is precised, with an implicit discretization of the electric field in the definition of the sources for both the Ampere equation and the Gauss law, providing the consistency with the limit problem. Two implementation of the AP-methods are proposed, referred in the sequel as AP-Moment and AP-Particle schemes, both using a prediction, on the grid, of the Maxwell's system sources, but with a different discretization of the stress tensor.

Since the AP-methods are semi implicit schemes a survey of other implicit Particle-In-Cell schemes is provided in the section 4, without the purpose to be exhaustive, this topic being the subject of a very active research for tens of years. The derivation of these numerical methods all differ from the one introduced here, the implicit (or semi implicit) methods being developed in order to remove the most severe limitations on the discretization parameters. The methodology operated in the present work is completely different. The asymptotic preserving methods are constructed to join two models in a single numerical method. The improved efficiency of the AP-method is then secured by the consistancy with the limit regime in which the fastest scales are dropped out. The derivation proposed in this paper is a first step in developing numerical methods with more singular asymptotics and reduced limit models, to improve further the efficiency of the numerical method. A comparison with AP-methods design for the electrostatic framework [20] is also provided and the equivalence of the AP-Moment and AP-Particle schemes with these numerical methods in the electrostatic regime is stated.

Finally, in the section 5, the capabilities of these introduced schemes are investigated thanks to various and demanding numerical simulations. The first test cases are related to electrostatic configurations, with the classical Lamdau damping implemented to assess the efficiency of the AP-methods for the description of phenomena occuring at the Debye length and the plasma period. A more demanding test case is thus produced, relating the expansion of a plasma in the vacuum. The physiscs into play is complex, with the creation of a non quasi-neutral sheath at the plasma boundary with the vacuum. This framework is also interesting with respect to the total energy conservation of the schemes, this expansion being characterized by the conversion of electron thermal energy into ionic kinetic energy via the electrostatic field. This process can not be well accounted for without a good total energy conservation of the numerical methods. The second series of test cases is devoted to electromagnetic configurations with the simulation of Plasma Opening Switches (POS). These devices operating rely on the interaction of an electro-magnetic wave with a dense plasma. The simulation of these POS is very challenging, necessitating to account for transitions between

vacuum areas, non quasi-neutral and quasi-neutral regions, with the propagation of the electromagnetic wave at the speed of light, its reflection and transmission by the plasma. This device is first simulated with a simplified one dimensional model, which makes possible to confront the outputs of the AP-schemes to reference solutions carried out thanks to standard methods. A four dimensional (in phase space) implementation is finally proposed to reproduce a Magneto-Hydro-Dynamic non linear phenomenon; the so-called KMC wave explaining the propagation of the magnetic field into the plasma by means of a shock wave.

2 Quasi-neutral limit of the Vlasov-Maxwell system and its reformulation

2.1 Scope of the section

The Vlasov-Maxwell system is introduced in this section with the definition of the quasi-neutral regime examined in this paper. With this aim, the set of equations is re-scaled thanks to dimensionless variables, the quasi neutral regime being recovered for vanishing λ, a dimensionless parameter representing, among other dimensionless parameters, the ratio of the Debye length and the typical space scale of interest. This asymptotic parameter quantifies how close to quasi-neutrality the system is observed. The singular nature of the quasi-neutral limit is then highlighted, emphasizing the difficulty to handle this regime for numerical methods, owing to the degeneracy of the Ampere equation and the Gauss law. The difficulty of the quasi-neutral limit stems from the computation of the electric field in this regime. However, a set of equations defining the electric field in the quasi-neutral limit can be worked out. The derivation of this system, referred to as the limit problem in the sequel, is then detailed. Finally, a reformulated system is proposed, this set of equations, totally equivalent to the Vlasov-Maxwell system, is manufactured in order to turn the quasi-neutral limit into a regular perturbation problem, the limit problem being recovered from the reformulated system when λ goes to zero.

2.2 The Generalized Vlasov-Maxwell system

For simplicity, the ions are supposed to form a motionless and uniform background density, denoted by n_i. The electron evolution is described thanks to a distribution function f depending on the space variable $x \in \Omega_x \subset \mathbb{R}^3$, the microscopic velocity $v \in \Omega_v \subset \mathbb{R}^3$ and the time $t \in \mathbb{R}^+$. The electron density n, the electrical charge and current densities, ρ and J, are defined from the distribution function by

$$n = \int_{\mathbb{R}^3} f(x,v,t)\ dv, \quad \rho = e(n_i - n), \quad J = -e\int_{\mathbb{R}^3} f(x,v,t)v\ dv\,,$$

e denoting the elementary charge. We also define the second-order moment

$$S = \int_{\mathbb{R}^3} f(x,v,t)v \otimes v\ dv.$$

The distribution function f satisfies the Vlasov equation

$$\partial_t f + v\cdot\nabla_x f - \frac{e}{m}(E + v\times B)\cdot\nabla_v f = 0, \tag{1}$$

where m is the electron mass, E the electric field, and B the magnetic field. The electric and magnetic fields are created by the particles (self-consistent fields) and satisfy the following Maxwell equations:

$$\frac{1}{c^2}\partial_t E - \nabla\times B = -\mu_0 J, \tag{2}$$

$$\partial_t B + \nabla\times E = 0, \tag{3}$$

$$\nabla\cdot E = \frac{\rho}{\epsilon_0}, \tag{4}$$

$$\nabla\cdot B = 0, \tag{5}$$

where c is the speed of light, μ_0 the vacuum permeability, and ϵ_0 the vacuum permittivity. Of course, the above equations must be supplemented with initial and boundary conditions. The set up being test-case specific, both the boundary and the initial conditions will be precised in section 5 devoted to numerical simulations.

The Maxwell-Gauss equation (4) is actually an outcome of the Maxwell-Ampere equation (2) and the continuity equation

$$\partial_t \rho + \nabla \cdot J = 0$$

which translates the conservation of the electron and ion densities. Computing formally the divergence of the Maxwell-Ampere equation together with the continuity equation yields to

$$\partial_t \nabla \cdot E = \frac{1}{\epsilon_0} \partial_t^2 \rho \,,$$

meaning that, for the continuous system, the Maxwell-Gauss equation is satisfied for $t > 0$ as soon as it is satisfied for the initial condition. However, this property is not necessarily preserved by the discretization. In particular, for standard Particle-In-Cell methods, the source terms of the Maxwell equations, namely J and ρ, accumulated from particles do not satisfy the continuity equation. Consequently, the Gauss law is not verified, which can be the source of non-physical results in the numerical simulations, as pointed out in [6, 3]. Different procedures are succesfully used to correct this deficiency. A good review of which being detailed in [6]. Two main approaches can be identified. The first one consists in computing a correction generally applied to the electric field, this corrector being the solution of an elliptic, a diffusion or an elliptic equation. The second approaches rely on a modified particle projection in order to define a charge and a current density satisfying a discrete continuity equation on the grid. In the perspective to design a numerical method compliant with the quasi-neutral limit it is interesting to put the focus on the first kind on approaches and more specifically on the elliptic correction which implements the Gauss law for the corrector computation. Indeed this equation degenerates in the quasi-neutral limit, therefore a way to circumvent this difficulty needs to be provided.

To address this question the "generalized" Maxwell system will be considered in the sequel. In this modified set of equations, the Gauss law is explicitly enforced by means of a Lagrange multiplier, denoted p, associated to the divergence constraints of the electric field. One formulation of this system [4] reads:

$$\begin{aligned}
&\partial_t E - c^2 \nabla \times B - \nabla p = -\frac{J}{\epsilon_0} \,, \\
&\partial_t B + \nabla \times E = 0, \\
&\nabla \cdot E = \frac{\rho}{\epsilon_0}, \\
&\nabla \cdot B = 0 \,,
\end{aligned}$$

which is a well-posed set of equations equivalent to the standard Maxwell system [4]. The Lagrange multiplier verifies the following equation

$$-\Delta p = \frac{1}{\varepsilon_0} \left(\partial_t \rho + \nabla \cdot J \right)$$

and hence, vanishes as soon as the continuity equation is verified. Note that, up to the choice of an initial condition equal to zero for p and a change of variable, the augmented system can be recast into

$$\begin{aligned}
&\partial_t E - c^2 \nabla \times B = -\frac{J}{\epsilon_0} \,, \\
&\partial_t B + \nabla \times E = 0, \\
&\nabla \cdot \tilde{E} = \frac{\rho}{\epsilon_0}, \\
&\nabla \cdot B = 0 \,, \\
&\tilde{E} = E - \nabla p \,.
\end{aligned}$$

In this formulation, the electric field E is first advanced by means of the Ampere's law, then corrected, producing $\tilde{E}$, thanks to the correction carried out by the Gauss law. This procedure is referred to as the Boris correction [7].

Finally, the generalized Vlasov-Maxwell system amounts to the following set of equations

$$\partial_t f + v \cdot \nabla_x f - (\tilde{E} + v \times B) \cdot \nabla_v f = 0\,, \tag{6}$$

$$\partial_t E - c^2 \nabla \times B = -\frac{J}{\epsilon_0}\,, \tag{7}$$

$$\partial_t B + \nabla \times E = 0, \tag{8}$$

$$\nabla \cdot \tilde{E} = \frac{\rho}{\epsilon_0}, \tag{9}$$

$$\nabla \cdot B = 0, \tag{10}$$

$$\tilde{E} = E - \nabla p, \tag{11}$$

2.3 Scaling relations

The goal of this section is to exhibit the quasi-neutral limit of the system in a simple manner and more precisely the transition from the standard regime to the limit one by means of a vanishing dimensionless parameter. With this aim, the generalized Vlasov-Maxwell system (6)-(11) is rewritten thanks to dimensionless variables. Let x_0 and t_0 be the typical space and time scales of the targeted phenomena, n_0 the typical plasma density (assumed to be that of the ions $n_0 = n_i$), so that the typical values for the velocity, the distribution function as well as the charge and current densities, denoted by v_0, f_0, ρ_0 and J_0 are defined as

$$v_0 = \frac{x_0}{t_0}\,, \quad f_0 = \frac{n_0}{v_0}\,, \quad \rho_0 = e n_0\,, \quad J_0 = e n_0 v_0\,.$$

We also introduce dimensionless parameters: the dimensionless Debye Length λ, the Mach number M, the ratio of the electric and drift energies η, the typical velocity to the speed of light α, and β the ratio of the induction electric field to the typical electric field. These parameters write:

$$\lambda = \frac{\lambda_D}{x_0}, \quad M = \frac{v_0}{v_{th,0}}\,, \quad \eta = \frac{e x_0 E_0}{m v_0^2}\,, \quad \alpha = \frac{v_0}{c}, \quad \beta = \sqrt{\frac{v_0 B_0}{E_0}}\,,$$

where, $v_{th,0}$ is the typical electron thermal (or microscopic) velocity, (E_0, B_0) the characteristic value of the electromagnetic field, the Debye length λ_D and the plasma period τ_p verifying

$$\tau_p = \sqrt{\frac{m\epsilon_0}{e^2 n_0}}\,, \quad \lambda_D = \tau_p\, v_{th,0}\,.$$

Finally, the correction scale is deduced from that of the electric field with $p_0 = x_0 E_0$. Denoting, for simplicity, the scaled variables as the previous ones, the scaled generalized Vlasov-Maxwell system reads:

$$\begin{aligned}
&\partial_t f + \frac{1}{M} v \cdot \nabla_x f - \eta(\tilde{E} + \frac{\beta^2}{M} v \times B) \cdot \nabla_v f = 0\\
&\lambda^2 \eta M(\alpha^2 \frac{\partial E}{\partial t} - \beta^2 \nabla \times B) = -\alpha^2 J,\\
&\beta^2 \partial_t B + \nabla \times E = 0,\\
&\lambda^2 \eta M \nabla \cdot \tilde{E} = 1 - n,\\
&\nabla \cdot B = 0\,,\\
&\tilde{E} = E - \nabla p\,.
\end{aligned}$$

In order to reduce the number of parameters occurring in the above system, we have to choose how the parameters λ, η, M, α, and β scale with respect to each other. First, the drift and the thermal energies

are assumed to be the same order of magnitude and comparable to the electric energy, which translates into $M = \eta = 1$. The scaled Vlasov-Maxwell system reduces then to

$$\begin{aligned}
&\partial_t f + v \cdot \nabla_x f - \eta(\tilde{E} + \beta^2 v \times B) \cdot \nabla_v f = 0 \\
&\lambda^2\alpha^2 \frac{\partial E}{\partial t} - \lambda^2\beta^2 \nabla \times B = -\alpha^2 J, \\
&\beta^2 \partial_t B + \nabla \times E = 0, \\
&\lambda^2 \nabla \cdot \tilde{E} = 1 - n, \\
&\nabla \cdot B = 0\,, \\
&\tilde{E} = E - \nabla p\,.
\end{aligned}$$

The quasi-neutrality of the plasma is reached for vanishing λ, the Maxwell-Gauss law providing thus $n = 1$. It remains to choose the behavior of the parameters α and β. The goal is to preserve as many terms as possible in the system in the quasi-neutral limit (when $\lambda \to 0$) to obtain the richest limit problem. Whatever the choice for α, the displacement current $\lambda^2\alpha^2 \frac{\partial E}{\partial t}$ remains small compared to the current of particles $-\alpha^2 J$ in the Ampere's law. Therefore, the less degeneracy requirement is met for $\alpha = \lambda$ and $\beta = 1$. The latter relation is the so-called "frozen field" assumption, conventionally used in Magneto-Hydro-Dynamic models, translating the property that, in a dense plasma, the magnetic field is convected with the plasma flow. In other words, the quasi-neutral regime is characterized by electromagnetic waves propagating with small velocities compared to the speed of light. The dimensionless Debye length being a small scale in the limit regime, we choose this single parameter for both scales and state thus $\alpha = \lambda$ to specify that the displacement current vanishes in the quasi-neutral limit. Finally we obtain the following system:

$$\partial_t f + v \cdot \nabla_x f - (\tilde{E} + v \times B) \cdot \nabla_v f = 0, \tag{12}$$
$$\lambda^2 \partial_t E - \nabla \times B = -J, \tag{13}$$
$$\partial_t B + \nabla \times E = 0, \tag{14}$$
$$\lambda^2 \nabla \cdot \tilde{E} = 1 - n, \tag{15}$$
$$\nabla \cdot B = 0, \tag{16}$$
$$\tilde{E} = E - \nabla p. \tag{17}$$

Remark 2.1. *With the scaling assumption $\eta = M = 1$, the plasma period can be expressed as $\tau_p = \lambda t_0$. Thus, the parameter λ controls both the smallness of the Debye length with respect to the space scale of the problem and the smallness of the plasma period with respect to the time scale of the problem. This feature explains the property P2 stated in the introduction.*
Note that λ also represents the typical velocity of the system evolution relative to the speed of light. Strictly speaking, this is not an outcome of the scaling, but a means of deriving the limit regime thanks to the vanishing of a single dimensionless parameter, this velocities ratio being small in the quasi-neutral regime.

2.4 The Quasi-neutral regime

The quasi-neutral model is obtained formally by letting λ go to zero in the scaled system (12)-(16):

$$\partial_t f + v \cdot \nabla_x f - (\tilde{E} + v \times B) \cdot \nabla_v f = 0, \tag{18}$$
$$\nabla \times B = J, \tag{19}$$
$$\partial_t B + \nabla \times E = 0, \tag{20}$$
$$n = 1, \tag{21}$$
$$\nabla \cdot B = 0, \tag{22}$$
$$\tilde{E} = E - \nabla p\,. \tag{23}$$

The singular nature of the quasi-neutral limit is made obvious in the re-scaled system: both the Maxwell-Gauss and the Maxwell-Ampere equations degenerate (compare (21) with (15) and (19) with (13)). This latter equation allows for the computation of the electric field in standard numerical methods discretizing the Vlasov-Maxwell system (1)-(5). In the quasi-neutral limit, the electric field being dropped in this equation, another equation needs to be worked out to advance this quantity. This remark also applies for the computation of the electric field correction p, in the generalized system.

Precisely, we note that the inductive part of the electric field can be carried out by the degenerated problem (18)-(22). Indeed taking the time derivative of equation (19) together with the curl of equation (20) yields

$$\nabla \times \nabla \times E = -\partial_t J \,, \tag{24}$$

which provides a means of computing the electric field solenoidal part. However, in (24) the electric field can be augmented by any gradient of a scalar function which proves that the electrostatic part of the electric field cannot be determined by this only equation. In the quasi-neutral regime, the electric field has to be computed from macroscopic equations (*ie* computed as the moment of kinetic objects), namely the conservation of the charge and current densities [38, 24, 17, 21, 5, 20, 29].

Following the Boris procedure the computation of the electric field is decomposed in two steps. First a prediction of this quantity is carried out using the Ampere's law. Second, the correction is computed by means of the Gauss law. The moments of the Vlasov equation give rise to the following equations

$$\partial_t n - \nabla \cdot J = 0 \,, \tag{25}$$

$$\partial_t J - \nabla \cdot S - nE + J \times B = 0 \,. \tag{26}$$

These definitions of the Maxwell's system sources are used for the computation of the electric field in the quasi-neutral regime. Precisely, inserting the definition of the current time derivative (26) into the equation (24), allows for the computation of the entire electric field in the quasi-neutral limit, thanks to

$$n\,E + \nabla \times \nabla \times E = J \times B - \nabla \cdot S. \tag{27}$$

Note that, in this asymptotic regime, the current density is genuinely divergence free if this property holds at the initial time. Indeed, denoting $\nabla^2 : S$ the contracted product of the Hessian with the tensor S, the equation (26) provides

$$\partial_t \nabla \cdot J = \nabla^2 : S + \nabla \cdot (nE) - \nabla \cdot (J \times B) \,. \tag{28}$$

The right hand side of this equation is the divergence of the reformulated Ampere's law (27), which proves that the current density remains divergence free. The continuity equation is thus satisfied as soon as $\partial_t^2(1 - n) = 0$. In this regime, the corrector p is therefore computed to enforce this constraint and prevent the particles to depart from the quasi-neutral balance $n = 1$.

To derive the equation satisfied by p, the starting point is the time derivative of the degenerated Gauss law (21) but with sources incorporating the contribution of the correction and defined as

$$\partial_t \tilde{n} - \nabla \cdot \tilde{J} = 0 \,, \qquad \partial_t \tilde{J} - \nabla \cdot S - n\tilde{E} + J \times B = 0 \,.$$

The correction is thus computed to enforce the constraint

$$\partial_t^2 \tilde{n} = 0 \,, \tag{29}$$

which finally gives the following elliptic equation for p

$$-\nabla \cdot (n \nabla p) = \nabla^2 : S + \nabla \cdot (nE) - \nabla \cdot (J \times B) \,.$$

In this equation, E is the predicted electric field, provided by (27) which together with the equations (25) and (26) gives rise to the following identity

$$\nabla \cdot (n \nabla p) = \partial_t^2 n \,.$$

This last equation outlines that, in the quasi-neutral regime too, the correction vanishes as soon as the continuity equation is satisfied. This finally gives rise to the definition of the limit problem.

Definition 2.1. *The quasi-neutral Generalized Vlasov-Maxwell system is defined as*

$$\partial_t f + v \cdot \nabla_x f - (\tilde{E} + v \times B) \cdot \nabla_v f = 0, \tag{30}$$
$$nE + \nabla \times \nabla \times E = J \times B - \nabla \cdot S, \tag{31}$$
$$\partial_t B + \nabla \times E = 0, \tag{32}$$
$$-\nabla \cdot (n \nabla p) = -\partial_t^2 n\,, \tag{33}$$
$$\nabla \cdot B = 0\,, \tag{34}$$
$$\tilde{E} = E - \nabla p\,. \tag{35}$$

Remark 2.2. *The rigorous derivation of the quasi-neutral limit for the Vlasov-Maxwell system, i.e. the convergence of the solutions of the Vlasov-Maxwell system (12)-(15) to a solution of the quasi-neutral Vlasov-Maxwell system (30)-(35) (with $p \equiv 0$) when $\lambda \to 0$, is an open problem. Even for the simpler Vlasov-Poisson system, few results exist; see for instance the introduction of [29] for a review.*

2.5 Reformulation of the generalized Vlasov-Maxwell system

The present objective is to manufacture a set of equations, equivalent to the original system (12)-(17), in which the limit $\lambda \to 0$ is regular, meaning that the quasi-neutral model defined by equations (30)-(35) is recovered when λ is set to zero in this reformulated system. This is the aim of the following result.

Proposition 2.1. *The reformulated Generalized Vlasov-Maxwell system defined as*

$$\partial_t f + v \cdot \nabla_x f - (\tilde{E} + v \times B) \cdot \nabla_v f = 0 \tag{36}$$
$$\lambda^2 \partial_t^2 E + nE + \nabla \times (\nabla \times E) = J \times B - \nabla \cdot S, \tag{37}$$
$$\partial_t B + \nabla \times E = 0, \tag{38}$$
$$-\lambda^2 \partial_t^2 \Delta p - \nabla \cdot (n \nabla p) = -\partial_t^2 n + \nabla^2 : S + \nabla \cdot (nE) - \nabla \cdot (J \times B), \tag{39}$$
$$\nabla \cdot B = 0\,, \tag{40}$$
$$\tilde{E} = E - \nabla p\,. \tag{41}$$

is equivalent to the Generalized Vlasov-Maxwell system provided that the Gauss law is satisfied at initial time. Moreover the quasi-neutral limit is regular in this system: the quasi-neutral Generalized Vlasov-Maxwell system (30)–(35) is recovered when $\lambda \to 0$.

Proof. First, reproducing the derivation performed in the quasi-neutral regime but with an asymptotic parameter $\lambda > 0$ the following reformulated Ampere's law is obtained

$$\lambda^2 \partial_t^2 E + nE + \nabla \times \nabla \times E = J \times B - \nabla \cdot S\,.$$

The correction is carried out from the Gauss law, or more precisely

$$-\lambda^2 \partial_t^2 \Delta p = -\partial_t^2 \tilde{n} - \lambda^2 \partial_t^2 \nabla \cdot E\,,$$

with

$$\partial_t^2 \tilde{n} = \partial_t^2 n - \nabla \cdot (n \nabla p)\,,$$

$\partial_t^2 n$ being defined thanks to the moments of the Vlasov equation (25) and (26). Thanks to the reformulated Ampere's law (37), the equation (39) is obtained for the corrector.

Second, we note that the reformulated quasi-neutral Ampere equation (31) is recovered from the equation (37) by setting $\lambda = 0$. In this limit, the correction satisfies

$$-\nabla \cdot (n \nabla p) = -\partial_t^2 n + \nabla^2 : S + \nabla \cdot (nE) - \nabla \cdot (J \times B)\,,$$

with a reformulated Ampere equation (37) providing

$$\nabla \cdot (nE) - \nabla \cdot (J \times B) + \nabla^2 : S = 0\,.$$

In the end, the equation (33) of the limit problem is obtained for the correction p. □

Note that, in contrast to (18)-(22), this reformulated system is suitable for a numerical approximation since the electric field E as well as the correction p are determined by (37) and (39) which are well posed equations, regardless of the asymptotic parameter values.

3 Asymptotic-preserving time-integration schemes

In the previous part, we have converted the Vlasov-Maxwell system into a system that does not degenerate in the quasi-neutral limit. Relying on this reformulation, we can derive the Asymptotic-Preserving schemes. Several space discretizations are possible for the fields: finite differences, finite volumes or finite elements. Herein, we choose a finite difference approximation on a regular rectilinear grid. For simplicity, the space domain is assumed to be a rectangular parallelepiped with periodic boundary conditions. Various interpolation and accumulation procedures exist for the Particle-In-Cell methos [6, 32]: nearest grid point, cloud-in-cell, etc.... They are all compatible with the Asymptotic-Preserving schemes described in this part. The numerical simulations reported in the sequel are performed with the cloud-in-cell procedure.

3.1 Definitions, notations, reference schemes

3.1.1 Discrete fields and discrete vector calculus operators

We consider different kinds of discrete fields on the regular rectilinear grid: primal and dual scalar fields, edge scalar field, primal and dual vector fields, primal symmetric second-order tensor field.

- The values of a primal scalar field are located at the vertices of the cells, while the values of a dual field are located at the centers of the cells. The values of an edge scalar field are located at the center of the edges.
- The components of a primal vector field are located at the center of the edges: the x-, y-, and z-components are located at the edges oriented in the x-, y-, and z-direction, respectively. The components of a dual vector field are located at the center of the faces: the x-, y-, and z-components are located at the faces normal to the x-, y-, and z-direction, respectively.
- The diagonal components of a primal symmetric second-order tensor field are located at the vertices of the grid. The xy-, xz- and yz-components are located at the center of the faces normal to the x-direction, y-direction, and z-direction, respectively.

Discrete differential operators can be defined on the discrete fields defined above by using central finite differences (and assuming periodic boundary conditions).

- A discrete curl operator $\nabla_h\times$ is defined for the primal and dual vector fields. When applied to a primal vector field (resp. dual vector field), the discrete curl operator yields a dual vector field (resp. primal vector field). Furthermore, if F_h is a primal vector field and G_h a dual vector field, then

$$\nabla_h \times F_h \cdot G_h - \nabla_h \times G_h \cdot F_h = 0. \tag{42}$$

- A discrete divergence operator $\nabla_h\cdot$ is defined for the primal and dual vector fields. When applied to a primal vector field (resp. a dual vector field), the discrete divergence operator yields a primal scalar (resp. a dual scalar field). If F_h is a primal or a dual field, then

$$\nabla_h \cdot (\nabla_h \times F_h) = 0. \tag{43}$$

- A discrete gradient operator ∇_h is defined for the primal and dual scalar fields. When applied to a primal sacalar field (resp. a dual scalar field), the discrete gradient operator yields a primal vector (resp. a dual vector field).
- A discrete divergence operator $\nabla_h \cdot$ is defined for the primal tensor field. It yields a primal vector field.

A discrete cross product approximating the cross product of primal vector field and an dual vector field as a primal vector field is also needed. Such a discrete operator can be built using local averages; it is noted $\times_h$.

3.1.2 Notation

- The grid spacing in the x-, y-, and z-direction are denoted by Δx, Δy, and Δz, respectively. Let $h := 1/\sqrt{\frac{1}{\Delta x^2} + \frac{1}{\Delta y^2} + \frac{1}{\Delta z^2}}$.
- The time interval is discretized with a uniform time step Δt. Let $t^\gamma := \gamma \Delta t$, where $\gamma \in \mathbb{R}_+$.
- The discrete electric and magnetic fields at time t^γ are denoted by E_h^γ and B_h^γ. The discrete electric field is a primal vector field while the discrete magnetic field is dual vector field. The discrete current at time t^γ is denoted by J_h^γ; it is a primal vector field.
- For a field F_h we set $\bar{F}_h^{m+\theta} := \theta F_h^{m+1} + (1-\theta) F_h^m$, where $m \in \mathbb{N}$ and $\theta \in [0,1]$.
- Let N be the number of particles. The vectors containing the position and the velocity of the particles at time t^γ are denoted by X_N^γ and V_N^γ, respectively. The position and velocity vectors of the jth particle at time t^γ are denoted by $X_{N,j}^\gamma$ and $V_{N,j}^\gamma$, respectively.
- The value of a field F_h interpolated at the position $X_{N,j}$ is denoted by $F_h(X_{N,j})$.
- The discrete electron density accumulated from the particles at position X_N as a primal scalar field (resp. an edge scalar field) is denoted by $n_h(X_N)$ (resp. $\hat{n}_h(X_N)$). The discrete current accumulated from the particles of position X_N and velocity V_N as a primal vector field is denoted by $J_h(X_N, V_N)$. The discrete second-order moment accumulated from the particles of position X_N and velocity V_N as a primal tensor is denoted by $S_h(X_N, V_N)$.

3.1.3 Reference integration schemes

Usual explicit discretizations of the Vlasov-Maxwell system combine an explicit scheme for advancing the particles and a leap-frog discretization for the Maxwell equations [6, Chapter 15]. Here is a discretization using a Boris scheme for the particles :

$$\frac{X_{N,j}^{m+1} - X_{N,j}^m}{\Delta t} = V_{N,j}^{m+\frac{1}{2}}, \qquad \forall j \in \{1, \dots, N\}, \tag{44}$$

$$\frac{V_{N,j}^{m+\frac{1}{2}} - V_{N,j}^{m-\frac{1}{2}}}{\Delta t} = -\tilde{E}_h^m\left(X_{N,j}^m\right) - \frac{V_{N,j}^+ + V_{N,j}^-}{2} \times B_h^m(X_{N,j}^m), \qquad \forall j \in \{1, \dots, N\}, \tag{45}$$

$$\lambda^2 \frac{\tilde{E}_h^{m+1} - E_h^m}{\Delta t} - \nabla_h \times B_h^{m+\frac{1}{2}} = J_h(X_N^{m+1}, V_N^{m+\frac{1}{2}}), \tag{46}$$

$$\frac{B_h^{m+\frac{1}{2}} - B_h^{m-\frac{1}{2}}}{\Delta t} + \nabla_h \times E_h^m = 0, \tag{47}$$

$$\tilde{E}_h^{m+1} = E_h^{m+1} - \nabla_h p_h, \tag{48}$$

$$-\lambda^2 \Delta_h p_h = 1 - n_h(X_N^{m+1}) - \lambda^2 \nabla_h \cdot E_h^{m+1}, \tag{49}$$

where

$$V_{N,j}^{+} = V_{N,j}^{m+\frac{1}{2}} - \frac{1}{2}\Delta t E_h^m\left(X_{N,j}^m\right), \qquad \forall j \in \{1,\dots,N\}, \tag{50}$$

$$V_{N,j}^{-} = V_{N,j}^{m-\frac{1}{2}} + \frac{1}{2}\Delta t E_h^m\left(X_{N,j}^m\right), \qquad \forall j \in \{1,\dots,N\}, \tag{51}$$

$$B_h^m = \frac{1}{2}\left(B_h^{m-\frac{1}{2}} + B_h^{m+\frac{1}{2}}\right). \tag{52}$$

The equations are solved in the order (47), (45), (44), (46), (49), (48), so that the scheme is fully explicit. This scheme is subject to a number of constraints[1]. Firstly, the time step must resolve the plasma period:

$$\Delta t < 2\tau_p \qquad [\Delta t < 2\lambda t_0]. \tag{53}$$

The grid spacing must also resolve the Debye length,

$$h < \zeta\lambda_D \qquad [h < \zeta\lambda x_0], \tag{54}$$

where ζ is a parameter depending on the assignment-interpolation procedure. Otherwise, aliasing will heat up the plasma. And, finally,

$$v_{th}\frac{\Delta t}{h} < 1 \qquad \left[v_0\frac{\Delta t}{h} < 1\right]. \tag{55}$$

Furthermore, the discretization of the Maxwell equations with a leap-frog scheme introduces a Courant condition involving the speed of light. With Yee's finite difference discretization, this condition is [50]:

$$c\frac{\Delta t}{h} < 1 \qquad \left[\frac{\lambda}{v_0}\frac{\Delta t}{h} < 1\right]. \tag{56}$$

Because of the stability conditions (53) and (54), the above explicit discretization is unstable in the quasi-neutral limit. Therefore, it does not satisfy the condition P2, and hence is not Asymptotic-Preserving.

To relax the Courant condition involving the speed of light, the Maxwell equations can be discretized with an implicit time-integration scheme while keeping explicit sources. Various implicit schemes for the Maxwell equations have been considered in the literature (see [2, 8, 10] for instance). Here we use a θ-scheme, whose main properties are recalled in Appendix A. The equations (45) and (46) are then substituted by

$$\lambda^2\frac{E_h^{m+1} - E_h^m}{\Delta t} - \nabla_h \times \bar{B}_h^{m+\theta} = -J_h(X_N^{m+1}, V_N^{m+\frac{1}{2}}), \tag{57}$$

$$\frac{B_h^{m+1} - B_h^m}{\Delta t} + \nabla_h \times \bar{E}_h^{m+\theta} = 0. \tag{58}$$

with

$$\bar{E}_h^{m+\theta} = \theta E_h^{m+1} + (1-\theta)E_h^m, \qquad \bar{B}_h^{m+\theta} = \theta B_h^{m+1} + (1-\theta)B_h^m$$

The above discretization is still subject to the stability conditions (53) and (54), and hence is not Asymptotic-Preserving.

3.2 Asymptotic-preserving time-integration schemes

3.3 Introduction

Let us consider the first-order Maxwell equations (13)-(14) supplemented with the moment equations (25)-(26). Our aim is to discretize in time these equations so that the discrete problem is consistent with the Vlasov-Maxwell system when $\lambda = \mathcal{O}(1)$ and with the quasi-neutral regime for $\lambda \ll 1$ with no restrictions on the discretization parameters related to λ. The investigations performed on the continuous system show that:

[1]The stability conditions are given both with the physical parameters and the scaling parameter λ.

1. the homogeneous part of the Maxwell equations (with null source terms) must be discretized with an implicit time-integration scheme to meet property P2;

2. the sources J and n in the Ampere's and Gauss laws must be approximated with an implicit electric field in order to secure a means of computing the electric field and the correction in the quasi-neutral regime and satisfy property P3.

To discretize implicitly the Maxwell equations, we choose the θ-scheme (with $\theta \geq \frac{1}{2}$), with an electric field made implicit in the definition of the current density, precisely

$$\lambda^2 \frac{E_h^{m+1} - E_h^m}{\Delta t} - \nabla_h \times \bar{B}_h^{m+\theta} = -J_h^{m+1}, \tag{59}$$

$$\frac{B_h^{m+1} - B_h^m}{\Delta t} + \nabla_h \times \bar{E}_h^{m+\theta} = 0. \tag{60}$$

$$\lambda^2 \nabla_h \cdot \left(E_h^{m+1} - \nabla_h p\right) = 1 - \tilde{n}_h^{m+1}\,, \tag{61}$$

The current $J_h^{m+\theta}$ used as the source of the Ampere equation will be defined with an implicit electric field:

$$J_h^{m+1} = J_h^{m,\star} + \Delta t\, \hat{n}_h(X_N^m) E_h^{m+1} \tag{62}$$

where $J_h^{m,\star}$ is an explicit component. The definition and the computation of this quantity will be detailed in the next two sections. The charge density $\tilde{n}_h^{m+1}$ is constructed thanks to the corrected implicit electric field, with

$$\tilde{n}^{m+1} = n_h(X_N^m) + \Delta t \nabla_h \cdot \tilde{J}_h^{m+1}\,, \qquad \tilde{J}_h^{m+1} = J_h^{m,\star} + \Delta t\, \hat{n}_h(X_N^m)\, \tilde{E}_h^{m+1}\,.$$

Finally the time discretized reformulated Generalized Vlasov-Maxwell system reads

$$\lambda^2 \frac{E_h^{m+1} - E_h^m}{\Delta t} - \nabla_h \times \bar{B}_h^{m+\theta} = -J_h^{m+1}\,, \tag{63}$$

$$\frac{B_h^{m+1} - B_h^m}{\Delta t} + \nabla_h \times \bar{E}_h^{m+\theta} = 0\,, \tag{64}$$

$$-\nabla_h \cdot \Big(\big(\lambda^2 + \Delta t^2 \hat{n}_h(X_N^m)\big)\nabla_h p_h\Big) = 1 - n_h^{m+1} - \lambda^2 \nabla_h \cdot E_h^{m+1}\,, \tag{65}$$

$$J_h^{m+1} = J_h^{m,\star} + \Delta t\, \hat{n}_h(X_N^m) E_h^{m+1}\,, \tag{66}$$

$$n_h^{m+1} = n_h(X_N^m) + \Delta t \nabla_h \cdot J_h^{m+1}\,. \tag{67}$$

Note that the right hand side of the equation (65) evaluates the inconsistancy of the Gauss law for the predicted electric field. Using the equations (66) and (67) together with the divergence of the equation (63), the equation verified by the correction can be rewritten as

$$-\nabla_h \cdot \Big(\big(\lambda^2 + \Delta t^2 \hat{n}_h(X_N^m)\big)\nabla_h p_h\Big) = 1 - n_h^m(X_N^m) - \lambda^2 \nabla_h \cdot E_h^m\,.$$

The correction have the effect to prevent the growth, from time step to time step, of the inconsistancy between the electrostatic field and the charge density accumulated from particles.

The electric and magnetic fields are computed by solving the linear system which is obtained by eliminating $J_h^{m+\theta}$ in (63)-(64), yielding to

$$A_h^m Z_h^{m+1} = R_h^m \tag{68}$$

with $Z_h^{m+1} = (E_h^{m+1}, B_h^{m+1})^T$,

$$A_h^m Z_h^{m+1} := \begin{pmatrix} \Big(\lambda^2 + \Delta t^2 \hat{n}_h(X_N^m)\Big) E_h^{m+1} - \theta \Delta t \nabla_h \times B_h^{m+1} \\ B_h^{m+1} + \theta \Delta t \nabla_h \times E_h^{m+1} \end{pmatrix}, \tag{69}$$

$$R_h^m := \begin{pmatrix} \lambda^2 E_h^m + (1-\theta)\Delta t \nabla_h \times B_h^m - \Delta t J_h^{m,\star} \\ B_h^m - (1-\theta)\Delta t \nabla_h \times E_h^m \end{pmatrix}. \tag{70}$$

Lemma 3.1. *The linear system defined by* (68)-(69) *is unconditionally invertible. As a corollary, the reformulated Gauss law* (65) *is elliptic.*

Proof. Using the identity (42), we obtain

$$(Z_h^{m+1})^T A_h^m Z_h^{m+1} \geq \left(\lambda^2 + \Delta t^2 \min\left(\hat{n}_h(X_N^m)\right)\right) \|E_h^{m+1}\|^2 + \|B_h^{m+1}\|^2.$$

The coefficient $(\lambda^2/\Delta t^2) + \min\left(\hat{n}_h(X_N^m)\right)$ is expected to be always positive (when λ becomes small, the density $\hat{n}_h(X_N^m)$ is expected to be close to 1). Therefore, A_h^m is a definite positive matrix. □

The time advance of the particles and the computation of the current density remain to be precised. The particle pusher details are reported in appendix B. Two approaches are proposed in the following subsections. The first one is based on an Eulerian integration of the moment equations and will thus be referred to as "AP-Moment" method. The second one relies on the particle pusher, to avoid the space differentiation of the stress tensor, by integrating its contribution thanks to a Lagrangian scheme. This later scheme is thus named "AP-Particle" method in the sequel.

3.3.1 AP-Moment scheme

In this section, we derive the AP-Moment scheme which makes use of the Vlasov equation moment to construct the implicit equation providing the current density, with

$$\frac{J_h^{m+1} - J_h(X_N^m, V_N^m)}{\Delta t} - \nabla_h \cdot S_h(X_N^m, V_N^m) - \hat{n}_h(X_N^m)\bar{E}_h^{m+1} + J_h(X_N^m, V_N^m) \times_h B_h^m = 0. \tag{71}$$

Using the notation introduced in the equation (66), this amounts to the definition

$$J_h^{m,\star} = J_h(X_N^m, V_N^m) + \Delta t\Big(\nabla_h \cdot S_h(X_N^m, V_N^m) - J_h(X_N^m, V_N^m) \times_h B_h^m\Big) \tag{72}$$

The particle pusher consists of a Boris like scheme with an implicit (corrected) electric field, defined as follows

$$\frac{X_{N,j}^{m+1} - X_{N,j}^m}{\Delta t} = V_{N,j}^{m+1}, \qquad \forall j \in \{1, \dots, N\}, \tag{73}$$

$$\frac{V_{N,j}^{m+1} - V_{N,j}^m}{\Delta t} = -\tilde{E}_h^{m+1}\left(X_{N,j}^m\right) - \frac{V_{N,j}^+ + V_{N,j}^-}{2} \times B_h^m(X_{N,j}^m), \qquad \forall j \in \{1, \dots, N\}, \tag{74}$$

where

$$V_{N,j}^+ = V_{N,j}^{m+1} - \frac{1}{2}\Delta t \tilde{E}_h^{m+1}\left(X_{N,j}^m\right), \qquad \forall j \in \{1, \dots, N\}, \tag{75}$$

$$V_{N,j}^- = V_{N,j}^m + \frac{1}{2}\Delta t \tilde{E}_h^{m+1}\left(X_{N,j}^m\right), \qquad \forall j \in \{1, \dots, N\}. \tag{76}$$

Proposition 3.1. *The discrete system* (63)-(67) *together with the definiton* (72) *provides a consistent time discretization of the reformulated system* (36)-(40). *In the limit* $\lambda \to 0$, *the system* (63)-(67) *defines a consistent discretization of the quasi-neutral Generalyzed Vlasov-Maxwell system* (30)-(35).

Proof. First we note that, with $\theta = 1$ (to simplify the formulas), the system (68)-(69) yields to

$$\frac{\lambda^2}{\Delta t^2}\left(E^{m+1} - E^m\right) = \frac{1}{\Delta t}\Big(\nabla \times B^m - J_h^m(X_N^m, V_N^m)\Big) - \nabla_h \times \nabla_h \times E_h^{m+1} - \hat{n}_h(X_N^m)E_h^{m+1} - \nabla_h \cdot S_h^m + J_h^m(X_N^m, V_N^m) \times B_h^m\,. \tag{77}$$

The Ampere's law is assumed to be satisfied at the precedent time step, with

$$\nabla_h \times B_h^m - J_h^m(X_N^m, V_N^m) \approx \frac{\lambda^2}{\Delta t}\left(E_h^m - E_h^{m-1}\right),$$

so that the following approximation holds

$$\frac{\lambda^2}{\Delta t^2}\left(E_h^{m+1} - 2E_h^m + E_h^{m-1}\right) + \nabla_h \times \nabla_h \times E_h^{m+1} + \hat{n}_h(X_N^m)E_h^{m+1} + \nabla_h \cdot S_h^m - J_h^m(X_N^m, V_N^m) \times B_h^m \approx 0\,,$$

defining a consistent discretization of the reformulated Ampere's law (36).

Second, the equations (65) and (77) provide

$$-\nabla_h \cdot \Big(\big(\frac{\lambda^2}{\Delta t^2} + \hat{n}_h(X_N^m)\big)\nabla_h p_h\Big) = \frac{1}{\Delta t^2}\Big(1 - n_h^{m+1} - \lambda^2 \nabla_h \cdot E_h^m\Big)$$
$$\nabla_h \cdot J_h^m(X_N^m, V_N^m) + \nabla_h^2 : S^m - \nabla_h \cdot (J_h^m \times B^m) - \nabla_h \cdot (\hat{n}_h(X_N^m)E^{m+1})\,.$$

Assuming that the Gauss law as well as the continuity equations are satisfied at the preceding time step so that the following approximations hold

$$\lambda^2 \nabla_h \cdot E_h^m \approx 1 - n_h(X_N^m)\,,$$
$$\Delta t \nabla_h \cdot J_h^m(X_N^m, V_N^m) \approx n_h(X_N^m) - n_h(X_N^{m-1})\,,$$

the following equation can be stated

$$-\nabla_h \cdot \Big(\big(\frac{\lambda^2}{\Delta t^2} + n_h(X_N^m)\big)\nabla_h p_h\Big) \approx \frac{1}{\Delta t^2}\Big(-n_h^{m+1} + 2n_h(X_N^m) - \hat{n}_h(X_N^{m-1})\Big)$$
$$- \nabla_h^2 : S^m - \nabla_h \cdot (J_h^m \times B^m) - \nabla_h \cdot (\hat{n}_h(X_N^m)E^{m+1})\,,$$

which defines a time discretization of the reformulated Gauss law (39) provided that the correction at time level m and $m-1$ vanish.

The consistancy with the quasi-neutral regime is secured thanks to the implicit time discretization of the electric field in the definition of the current density. □

Remark 3.1. *The derivation of the continuous reformulated system* (36)-(40) *requires the time derivation of the Ampere's and the Gauss laws in order to pull new electric field contributions from the sources definition into these equations. For the discretized system the time discretization these derivations are substituted by implicit time discretizations. Consequently the assumptions made on the initial conditions to prove the consistancy property of proposition 3.1 are not necessary for the discrete system.*

3.3.2 AP-Particle scheme

An alternate formulation of the AP-scheme is proposed in this section. It consists in the following definition for the current density

$$\begin{aligned} J^{m+1} &\approx J^m + \int_{t^m}^{t^{m+1}} \int_{\mathbb{R}^3} (v \cdot \nabla_x f - (E + v \times B) \cdot \nabla_v f)\, v\, dv\, dt \\ &\approx J^m + \int_{t^m}^{t^{m+1}} \int_{\mathbb{R}^3} (v \cdot \nabla_x f - (v \times B) \cdot \nabla_v f)\, v\, dv\, dt + \Delta t\, \hat{n}_h(X_h^m)E^{m+1} \\ &\approx J_h(X_N^{m+1,\star}, V_N^{m+1,\star}) + \Delta t\, \hat{n}_h(X_h^m)E_h^{m+1}. \end{aligned}$$

The current density $J_h(X_N^{m+1,\star}, V_N^{m+1,\star})$ can be accumulated from the particles after a push from t^m to an intermediate state $t^{m+1,\star}$ constructed without any electric field contribution. This writes

$$\frac{X_{N,j}^{m+1,\star} - X_{N,j}^m}{\theta \Delta t} = V_{N,j}^{m+1,\star}, \qquad \forall j \in \{1, \dots, N\}, \tag{78}$$

$$\frac{V_{N,j}^{m+1,\star} - V_{N,j}^m}{\Delta t} = -V_{N,j}^m \times B_h^m(X_{N,j}^m), \qquad \forall j \in \{1, \dots, N\}. \tag{79}$$

This finally gives the following definition

$$J_h^{m,*} = J_h(X_N^{m+1,\star}, V_N^{m+1,\star}), \tag{80}$$

used to defined the current density (66).

Lemma 3.2. *The discrete system* (63)-(67) *together with the definitions* (78)-(81) *provides a consistent time discretization of the reformulated system* (36)-(40). *In the limit* $\lambda \to 0$, *the system* (63)-(67),(78)-(81) *defines a consistent discretization of the quasi-neutral Generalyzed Vlasov-Maxwell system* (30)-(35).

Proof. Note that when the number of particles is large, the following approximation is valid:

$$J_h(X_N^{m+1,\star}, V_N^{m+1,\star}) \approx J_h(X_N^m, V_N^m) - \Delta t \, \nabla_h \cdot S_h(X_N^m, V_N^m) + \Delta t J_h(X_N^m, V_N^m) \times B_h^m. \tag{81}$$

Therefore, the AP-Particle scheme shares the same consistancy properties than the AP-Moment scheme. □

Remark 3.2. *The AP-Particle scheme requires either two sets of particles or two pushes of the particles for a single time step.*

In practice, the scheme is solved in three steps. First, temporary copies of the particles are advanced to the position $X_N^{m+1,\star}$ and velocity $V_N^{m+1,\star}$ using (78)-(79). Then, the electric and magnetic fields are computed by solving the linear system (68)-(70). Finally, the particles are advanced to the position X_N^{m+1} and velocity V_N^{m+1} using the scheme (73)-(74).

4 Comparison with other implicit Particle-In-Cell methods

4.1 Fully implicit, Direct and Moment implicit methods

The Asymptotic preserving property requires some level of implicitness in order to secure the consistancy with the limit model and consequently to prevent the degeneracy of the equations providing the electric field. Indeed, from the Ampere equation, the electric field is classically advanced by means of the discretized displacement current (ie $1/c^2(\partial E/\partial t)$ in the equation (2)). This term vanishing in the quasi-neutral limit, another contribution of the electric field is operated for its computation. This new contribution is the origin of the implicitness of the AP-methods. Therefore, it is relevant to compare the approaches developed herein with other implicit methods. Numerous implicit methods have indeed been developed since the 1980s, with the aim to study large-scale phenomena. Explicit methods are not well suited in this context, because they require very fine discretizations, at the scale of the plasma parameters, and lead to prohibitive computational costs for the simulation of macroscopic quantities over large time laps (see [39] for a review). Theoretically, a fully implicit discretization of the Vlasov-Maxwell system guarantees the stability for any discretization parameters. Unfortunately, the resulting problem is a huge system of coupled nonlinear equations (the particle equations and the field equations) and is hardly tractable numerically for an electromagnetic model with a six dimensional phase space.

Recently, impressive realizations have nevertheless been achieved on fully implicit methods in [12, 42, 51]. In this series of works, the purpose is to alleviate the constraints on the mesh size and the time step by inverting the non linear field-particle system. In these methods, the only occurrence of the advanced electric field in the Ampere equation is limited to the discretized displacement current. At first sight, this

method may appear to fail to meet the AP property in the quasi-neutral limit. However, the implicit electric field is involved in the definition of the sources, so that, the asymptotic preserving property can therefore be recovered at the price of the non linear field-particle system resolution. This represents an important numerical cost circumscribed with difficulty for 1D-1V configurations, despite the use of elaborated preconditioner [14] and massively parallel computations [13].

Semi implicit methods operates a linearization of the system in order to explicitly introduce the advanced electric field in the Maxwell's equation sources, decoupling thus the field system from the particle equations. Again, the purpose of these methods is to derive numerical schemes with discretization parameters less constrained than explicit ones. Two implementation of this approach can be indentified: the Moment Implicit Method [44, 9, 53, 45, 46, 40, 43] and the Direct Implicit Method [37, 16, 15, 31]. The Moment Implicit Method harness the moments of the Vlasov equation to predict the sources of the Maxwell's equations evaluated with an implicit electro-magnetic field. In the spirit, this approach is similar to the one developed in this paper and seems compliant with the quasi-neutral regime. The linearization procedure implemented in the direct implicit method is different in its implementation. It consists of a linearization of the sources around an extrapolated position constructed thanks to explicit quantities. The field equations are thus approximated with linearized sources constructed thanks to expansion of the shape functions used to project the particle properties on the grid and is thus completely bounded to the PIC framework. Note that the method may be iterated in order to converge the coupled field-particle system. Although these two approaches are different in their spirit the linearized equations solved for the advanced electric field are very close. Discussions in [23, 37] try to analyze precisely in what extent they may differ, with a final conclusion stating that the main differences are explained by the linearization around an extrapolated state for the Direct method which is not implemented in its counterpart. Another dissimilarity comes from the computation of the stress tensor, whose contribution is integrated by the particles motion during the extrapolation phase in the Direct method while it is accumulated from particles on the grid and then integrated by means of an Eulerian discretization in the Moment approach. Therein, the AP-Particle scheme shares some analogies with the Direct Implicit Methods while the AP-Moment schemes is more similar to the Moment Implicit Method.

It also appears that, while the Direct method is promoted to be more straightforward because the linearization of the system is derived directly from the PIC shape functions without the need to use auxiliary moments equations [37, 31], the Moment approach fits better with the regimes and models transition as operated in the Asymptotic-Preserving methodology. Indeed, while the electric field is carried out by the Maxwell's equations in the standard regime, its evolution is driven by macroscopic equations (the continuity equation or the momentum conservation) in the quasi-neutral regime so that it definitely makes sense to construct the moment equations defining the limit model, as proposed by the Moment approach.

From these comparisons, we can infer that implicit or semi implicit methods may generally be Asymptotic-Preserving in the quasi-neutral limit. Nevertheless, given the diversity of the methods, only a case by case study may conclusively answer this question. However, as pointed out before (see the introduction), the methodology developed here departs from the main stream approaches based on the implicitation of PIC schemes in order to release the discretization parameters from the most severe stability constraints. In deriving an asymptotic preserving method, the effort is made on the models, and more specifically in the construction of a set of equations containing both regimes, a non trivial task when the asymptotic limit is singular. The reformulation step allows for the construction of a system containing both regimes with a smooth transition between them. In this set of equations, the consistancy requirements highlight the terms that need to be implicited in order to define a means of computing the quantities in one regime or the other. The efficiency of the AP-method, compared to explicit schemes, is then related to the complexity reduction of the limit problem, which should be a well posed set of equations for all the quantities advanced in the standard regime, but without the fastest scales. The quasi-neutral regime defined by the scaling relations stated in the section 2.3 is recovered for vanishing scaled Debye length and plasma period as well as a typical velocity small compared to the speed of light. These three scales are responsible of the most severe limitations on the discretization parameters of explicit schemes, which explains the similarities of the AP-methods and the semi-implicit schemes. However, the AP methodology makes possible the extension of this achievement to more singular asymptotics, implementing limit models with a more reduced complexity

and an improved efficiency for the numerical method thereby derived.

For completeness of the bibliographic analysis, we note also some variants in the implementation of the implicit Maxwell system, sometimes achieved thanks to a potential formulation [9, 45, 52] or considering a low frequency approximation, the Darwin approximation [30, 26].

4.2 AP-Moment and AP-Particle schemes in the electrostatic regime

In the electrostatic case, referring to a vanishing magnetic field, the electric field is irrotational as a consequence of the Maxwell-Faraday law ($\nabla \times E = 0$) and therefore assumed to derive from a potential accordingly to $E = -\nabla\phi$. In this regime, either the Ampere equation or the Gauss law is sufficient to determine the entire electric field. The Vlasov-Maxwell system reduces to the Vlasov-Poisson system which reads

$$\partial_t f + v \cdot \nabla_x f + \nabla\phi \cdot \nabla_v f = 0, \tag{82}$$

$$-\lambda^2 \Delta\phi = 1 - n\,. \tag{83}$$

In this section, the AP-schemes, introduced in the preceding sections, are examined in the electrostatic regime. Let ϕ_h^{m+1} and $\tilde{\phi}_h^{m+1}$ the potentials corresponding to E_h^{m+1} and $\tilde{E}_h^{m+1}$ which satisfy the identity

$$\nabla_h \tilde{\phi}_h^{m+1} = \nabla_h \phi_h^{m+1} + \nabla_h p_h,$$

so that we can state the following property:

Proposition 4.1. *In the electrostatic regime the AP-moment scheme reduces to*

$$\Big(\lambda^2 + \Delta t^2\ \hat{n}_h(X_N^m)\Big) E_h^{m+1} = \lambda^2 E_h^m - \Delta t \nabla_h \cdot J_h(X_N^m, V_N^m) - \nabla_h^2 : S_h(X_N^m, V_N^m)\,, \tag{84}$$

$$-\nabla_h \cdot \Big(\big(\lambda^2 + \Delta t^2 \hat{n}_h(X_N^m)\big)\nabla_h p_h\Big) = 1 - n_h(X_N^m) - \lambda^2 \nabla_h \cdot E_h^m\,, \tag{85}$$

$$\tilde{E}_h^{m+1} = E_h^{m+1} - \nabla_h p_h\,. \tag{86}$$

with the particles advanced thanks to

$$\frac{X_{N,j}^{m+1} - X_{N,j}^m}{\Delta t} = V_{N,j}^{m+1}, \qquad \forall j \in \{1, \dots, N\}, \tag{87}$$

$$\frac{V_{N,j}^{m+1} - V_{N,j}^m}{\Delta t} = -\tilde{E}_h^{m+1}(X_{N,j}^m), \qquad \forall j \in \{1, \dots, N\}. \tag{88}$$

In one dimensional spatial configuration, this scheme is equivalent to the PIC-AP2 scheme introduced in [20] and defined as

$$-\nabla_h \cdot \left(\left(\frac{\lambda^2}{\Delta t^2} + \hat{n}_h(X_N^m)\right) \nabla_h \tilde{\phi}_h^{m+1}\right) = \frac{1 - n_h(X_N^m)}{\Delta t^2} - \Delta t \nabla_h \cdot J_h(X_N^m, V_N^m) - \nabla_h^2 : S_h(X_N^m, V_N^m), \tag{89}$$

the particles being advanced thanks to (87)-(88).

A similar proposition holds for the AP-Particle scheme.

Proposition 4.2. *In the electrostatic regime, the AP-Particle scheme reduces to*

$$\Big(\lambda^2 + \Delta t^2 \theta^2\ \hat{n}_h(X_N^m)\Big) E_h^{m+1} = \lambda^2 E_h^m - \Delta t J_h(X_N^{m+1,\star}, V_N^{m+1,\star})\,, \tag{90}$$

$$-\nabla_h \cdot \Big(\big(\lambda^2 + \Delta t^2 \hat{n}_h(X_N^m)\big)\nabla_h p_h\Big) = 1 - n_h(X_N^m) - \lambda^2 \nabla_h \cdot E_h^m\,, \tag{91}$$

$$\tilde{E}_h^{m+1} = E_h^{m+1} - \nabla_h p_h\,, \tag{92}$$

where

$$V_N^{m+1,\star} = V_{N,j}^m \,, \tag{93}$$

$$\frac{X_{N,j}^{m+1,\star} - X_{N,j}^m}{\Delta t} = V_N^{m+1,\star}, \qquad \forall j \in \{1,\dots,N\}\,, \tag{94}$$

the particles being finally advanced thanks to (87)-(88)*. In one dimensional spatial configurations, the system* (90) - (91) *is equivalent to*

$$-\nabla_h \cdot \left(\left(\frac{\lambda^2}{\Delta t^2} + \hat{n}_h(X_N^m) \right) \nabla_h \tilde{\phi}_h^{m+1} \right) = \frac{1 - n_h(X_N^m)}{\Delta t^2} - \Delta t \nabla_h \cdot J_h(X_N^{m+1,\star}, V_N^{m+1,\star}), \tag{95}$$

Proof of propositions 4.1 and 4.2. Setting $B = 0$, the equations (65) – (70) give

$$\left(\lambda^2 + \Delta t^2 \ \hat{n}_h(X_N^m)\right) E_h^{m+1} = \lambda^2 E_h^m - \Delta t J_h^{m,*}\,, \tag{96}$$

$$-\nabla_h \cdot \left(\left(\lambda^2 + \Delta t^2 \hat{n}_h(X_N^m)\right) \nabla_h p_h \right) = 1 - n^{m+1} - \lambda^2 \nabla_h \cdot E_h^{m+1}\,, \tag{97}$$

$$J_h^{m+1} = J_h^{m,*} + \Delta t \hat{n}_h(X_N^m) \left(E_h^{m+1}\right)\,, \tag{98}$$

$$n_h^{m+1} = n_h(X_N^m) + \Delta t \nabla_h \cdot J_h^{m+1}\,, \tag{99}$$

$$\tilde{E}_h^{m+1} = E_h^{m+1} - \nabla_h p_h\,. \tag{100}$$

Inserting the definitions (99) and (98) of n^{m+1} and J_h^{m+1} into the equation (97) yields to

$$-\nabla_h \cdot \left(\left(\lambda^2 + \Delta t^2 \hat{n}_h(X_N^m)\right) \nabla_h p_h \right) = 1 - n_h(X_N^m) - \Delta t \nabla_h \cdot J_h^{m,*} - \left(\lambda^2 + \Delta t^2 \hat{n}_h(X_N^m)\right) \nabla_h \cdot E_h^{m+1}\,, \tag{101}$$

which, thanks to (96), gives (85) and (91).

As mentionned before, in the electrostatic regime, the Gauss law is sufficient to compute the entire electric field, so that the Maxwell-Ampere equation can be disregarded. Starting from equation (101) and assuming that the electric field E^{m+1} is irrotational, a condition always met in one dimensional spatial configuration, so that the identity $E^{m+1} = -\nabla \phi^{m+1}$ holds, we obtain

$$-\nabla_h \cdot \left(\left(\lambda^2 + \Delta t^2 \hat{n}_h(X_N^m)\right) \nabla_h (\phi_h^{m+1} + p_h) \right) = 1 - n_h(X_N^m) + \Delta t \nabla_h \cdot J_h^{m,*}\,,$$

giving rise to the equations (89) and (95) accordingly to the definitions of $J_h^{m,*}$. □

5 Numerical simulations

5.1 Introduction

In order to assess the efficiency of the AP schemes and investigate their properties, numerical simulations on various one-dimensional problems are performed. The first one is the classical Landau damping, the second one is the simulation of plasma expansion into the vacuum. In these applications the magnetic effects are disregarded, thus the numerical methods are investigated in the electrostatic regime addressed in the section (4.2). The electro-magnetic configurations are considered thanks to the simulation of plasma opening switches, first in a simplified quasi one dimensional framework, then in a two and a half spatial configuration.

5.2 Landau damping

This test case is devoted to the simulation of the classical Landau damping. The initial data consists of a plasma in a spatially homogeneous equilibrium with a weak perturbation. The return of the plasma towards the equilibrium state is simulated thanks to a standard explicit PIC (Std.) code implementing the Vlasov

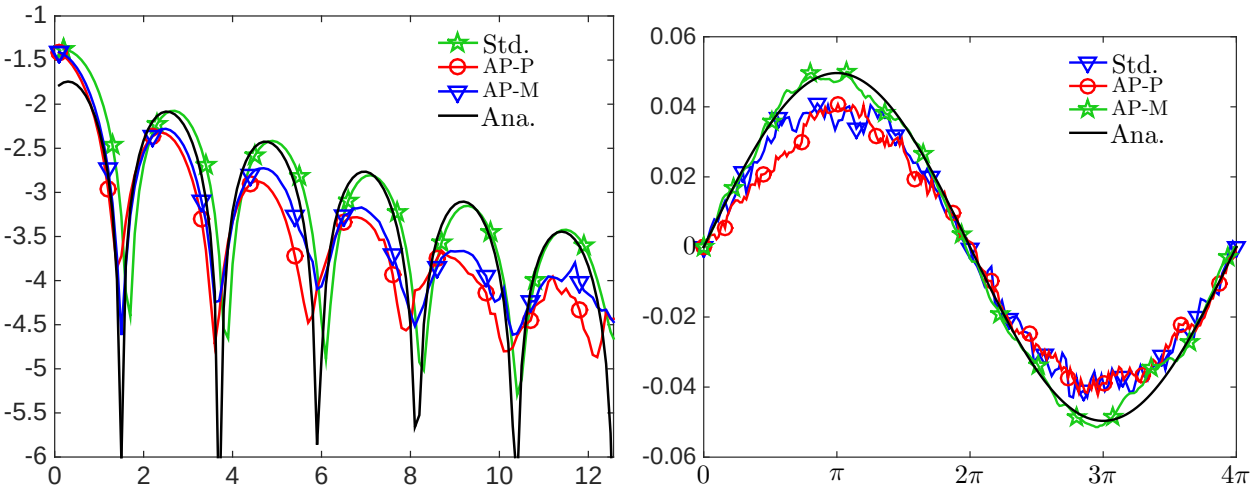

(a) Electric energy ($\|E_x\|$) as a function of time.

(b) Electric field as a function of x (t=2.5).

Figure 1: Landau damping. Time evolution of $\log(\|E_x\|)$ and electric field E_x at time $t = 2.5$ computed thanks to a standard explicit PIC method (Std.), the AP-Particle (AP-P) ans AP-Moment (AP-M) schemes and the analytic estimate (eq. (102)) on 250 cells ($\Delta x = 4\pi/2500 \sim \lambda_D/10$, $\Delta t = \tau_p/10$) with 10^6 particles.

Poisson system. This numerical solution is compared to that of the AP-Particle (AP-P) and AP-Moment (AP-M) schemes on the Figure 1. The test case is stated for the dimensionless system introduced in the section 2.4, the ions at rest, defining a uniform density background equal to one. The initial electron density follows a Maxwellian distribution with a small spatial perturbation, as defined by:

$$f_0(x,v) = \left(1 + \alpha \cos\left(\frac{x}{2}\right)\right) \frac{1}{\sqrt{2\pi}} e^{-\frac{v^2}{2}}, \tag{102}$$

where $\alpha = 5 \cdot 10^{-2}$. Periodic and homogeneous Dirichlet boundary conditions are prescribed for the particles and the electric field, respectively. A reference solution for the electric field can be computed by applying a Laplace-Fourier transform to the linearized equation (see [18] for the detailed calculation). Keeping only the dominating mode, the others being quickly damped, the electric field is given by

$$E_x^{\text{ref}}(x,t) = -1.4708\alpha e^{-0.1533t} \cos(1.4156t - 0.536245) \sin(x/2)\,. \tag{103}$$

One sees that the electric field decay is exponentially fast and is accompanied with oscillations whose period is close to the plasma period. The computations carried out by all the numerical methods produce comparable results as displayed on the figure 1. The AP-schemes are observed to introduce more damping, which may be explained by the implicitness of the time discretization. Indeed this damping can be dramatically reduced with lower time steps, which let envisioned that a higher order time discretization would improved significantly the damping properties of the AP-schemes. However these first numerical investigations demonstrate the ability of the AP methods to accurately account for phenomena occurring at the plasma period and the Debye length scales.

5.3 Plasma expansion

This test case is dedicated to the simulation of the expansion of a plasma slab into the vacuum as studied in [27, 20, 41]. The set of equations implemented for these numerical investigations is complemented with a

kinetic equation for the ions and writes (in dimensional units)

$$\partial_t f_e + v_x \cdot \partial_x f_e - \frac{e}{m_e} E_x \partial_{v_x} f_e = 0,$$
$$\partial_t f_i + v_x \cdot \partial_x f_i + \frac{e}{m_i} E_x \partial_{v_x} f_i = 0,$$
$$\partial_t E_x = -\frac{J_x}{\epsilon_0}, \quad \nabla \cdot E = \frac{\rho}{\epsilon_0}.$$

The plasma is initially confined in a small area at the center of the domain and surrounded by vacuum. During the expansion, the electrostatic interaction between electrons and ions converts progressively the thermal electron energy into ion kinetic energy, leading to an acceleration of the ions as depicted in Figures 2 and 3(b). This problem involves a plasma-vacuum interface with a transition fron the vacuum to a quasi-

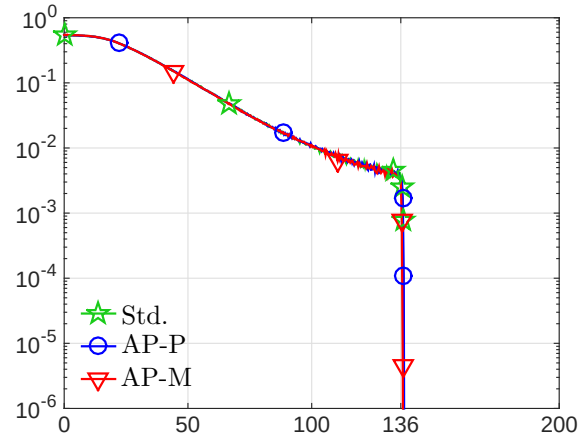

(a) Ionic density as a function of x.

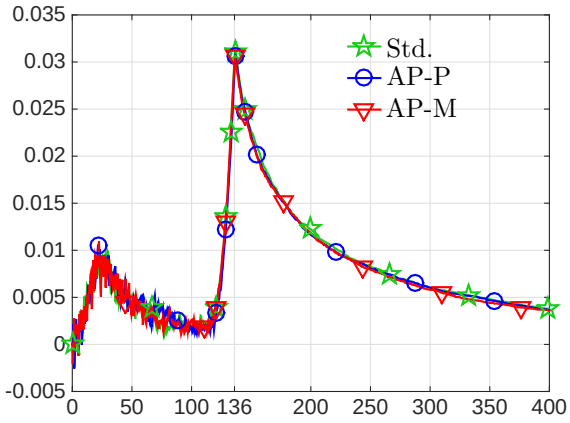

(b) Electric field as a function of x.

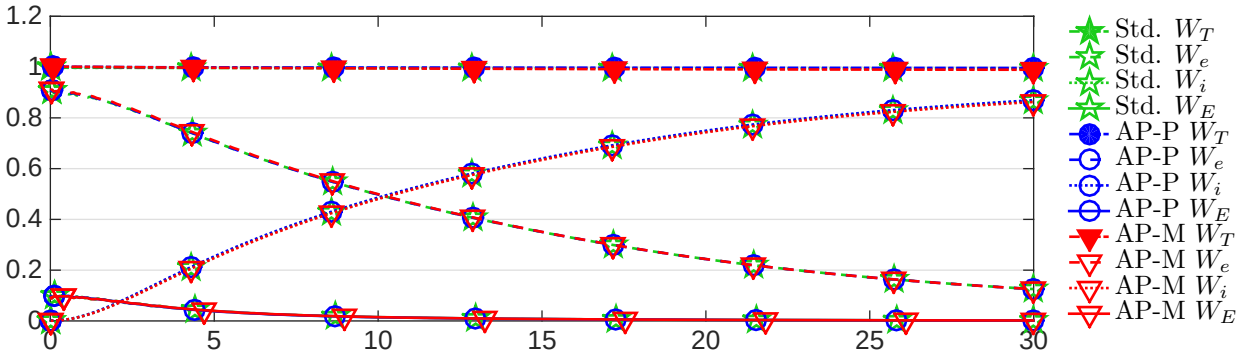

(c) Total (W_T), electronic (W_e), ionic (W_i) and electric (W_E) energies normalized by the initial total energy as functions of the normalized time (t/ω_{pi}).

Figure 2: Low density plasma expansion simulation on a refined mesh: normalized ionic density ($n_i/n_{i,0}$) and electric field (E/E_0, $E_0 = \sqrt{(n_0 k_B T_{e,0})/\epsilon_0}$) as functions of the normalized space variables (x/λ_D) at time $t = 30(\omega_{pi})^{-1}$ computed thanks to a standard explicit scheme (Std.) as well as the AP-M and the AP-P schemes with $\Delta x = 0.4\lambda_D$, $\Delta t = 0.5\tau_p$ and 10^6 particles for each species.

neutral area where the scales of interest are larger than the Debye length and the plasma period. To facilitate the comparisons, the first set up is the one used in [27, 20]. The half length of the domain is $L = 1$ and the half length of the initial confinement area is $L_0 = 2 \cdot 10^{-2}$. The electronic temperature is chosen so that

$v_{th,e} = 1$ with an ionic temperature verifying $T_i = 10^{-3}T_e$. The electron to ion mass ratio is set to 1836. For the simulations of the figure 2, the typical plasma density n_0 is adjusted to obtain a Debye length λ_D and a plasma period $\tau_p = \lambda_D/v_{th,e}$ equal to 10^{-3} (in their respective units). The initial ion density n_{i0} is uniform, equal to n_0 in the confinement area $x \in [0, L_0]$ and vanishes on the rest of the domain. The initial electron density n_{e0} verifies the Maxwell-Boltzmann relation $n_{e0} = n_0 \exp(\phi_0)$, where ϕ_0 is the electrostatic potential, solution of $-\Delta\phi_0 = e(n_{i0} - n_{e0})/\epsilon_0$. This non linear problem is solved numerically to construct the initial electronic density. The initial ion and electron velocities follow Maxwellian distributions with zero mean velocities. To represent the symmetry at the the left end of the half domain, a specular reflection condition is prescribed for the distribution functions (i.e. exiting particles are reinjected with reversed velocities)At the right end, an absorbing condition is enforced on the distribution functions (i.e. exiting particles are not reinjected).

The simulation results of the figure 2 are related to a mesh size and a time step smaller than the Debye length and the plasma period. The output provided by a standard discretization and the AP-schemes are very similar when the same mesh resolution is used. The position reached by the edge of the plasma is $x_T \sim 140\lambda_D$ which is in line with the simulations carried out in [27, 20]. This area is non quasi-neutral and exhibits a large electrostatic field created by the space charge, this electric field converting electron thermal energy into ionic drift energy as depicted by the energy balance history displayed on the figure 2(c). All the schemes are observed to produce computations with a good total energy conservation.

A second set of simulations is presented on the figure 3 and performed with a higher plasma density defining a Debye length and a plasma period equal to 10^{-4}. The purpose of these simulations is to demonstrate the ability of the AP-Schemes to produce accurate computations with a mesh that do not resolve the plasma parameters. The initial electron plasma density following the Maxwell-Boltzmann relation used in the precedent investigations is not well resolved on coarse meshes. To avoid the introduction of discrepancies in the scheme precision, the plasma density initialization used for ions is also applied to electrons. A reference solution is carried out thanks to the same standard explicit scheme, the AP-schemes being ran with a mesh size 10 to 25 times larger than the Debye length and with a time step either 2 or 5 times larger than the plasma period. Note also that the number of particles used for the AP-schemes is divided by 10 compared to the standard scheme, already ran with a reduced number of simulation particles as can be observed by the large oscillations on the plot of the figure 3(a). The use of a coarser mesh deterioriates the precision of the computations, but the AP methods furnish good estimations of the main system characteristics. The AP-Particle scheme is less diffusive than the AP-Moment and allows for a better tracking of the plasma-vacuum interface driving the plasma evolution, which in the end explains that, the AP-Particle scheme provides better simulation outputs than the AP-Moment one. With the coarsest mesh operated to produce these outputs, the energy conservation remains satisfactory, however the use of even coarser discretization parameters alter significantly the energy conservation of the method. This is a common weakness of semi-implicit schemes [23], that may be explained by fast particles crossing more than one cell in a time step. This point should be analyzed further in details in subsequent realizations.

5.4 Simulation of Plasma Opening Switches

5.4.1 Introduction and set up definition

A Plasma Opening Switch (POS) is a device used to deliver a large current with a rapid increase of its impedance [22]. It consists of a cylindrical-coaxial transmission line filled by a plasma with densities ranging from 10^{18} to 10^{22} and connected to an input power generator [54]. In a first phase, also referred to as the conduction phase, the plasma short-circuits the two electrodes of the transmission line and prevents the power to be delivered to the load. The operating of such a device relates on the interaction between a dense plasma and an electromagnetic wave which separates gradually the electrons from the ions, creating a non quasi-neutral sheath where the electrons are first expelled. The eclectrostatic field created by the charge density drives the ions out of the sheath, creating a vacum area [25, 47]. This device operating brings into play the interaction of an electro-magnetic wave with a dense plasma, transitions between vacuum, non quasi-neutral and quasi-neutral regions with time evolving interfaces. These multi-physics phenomena are

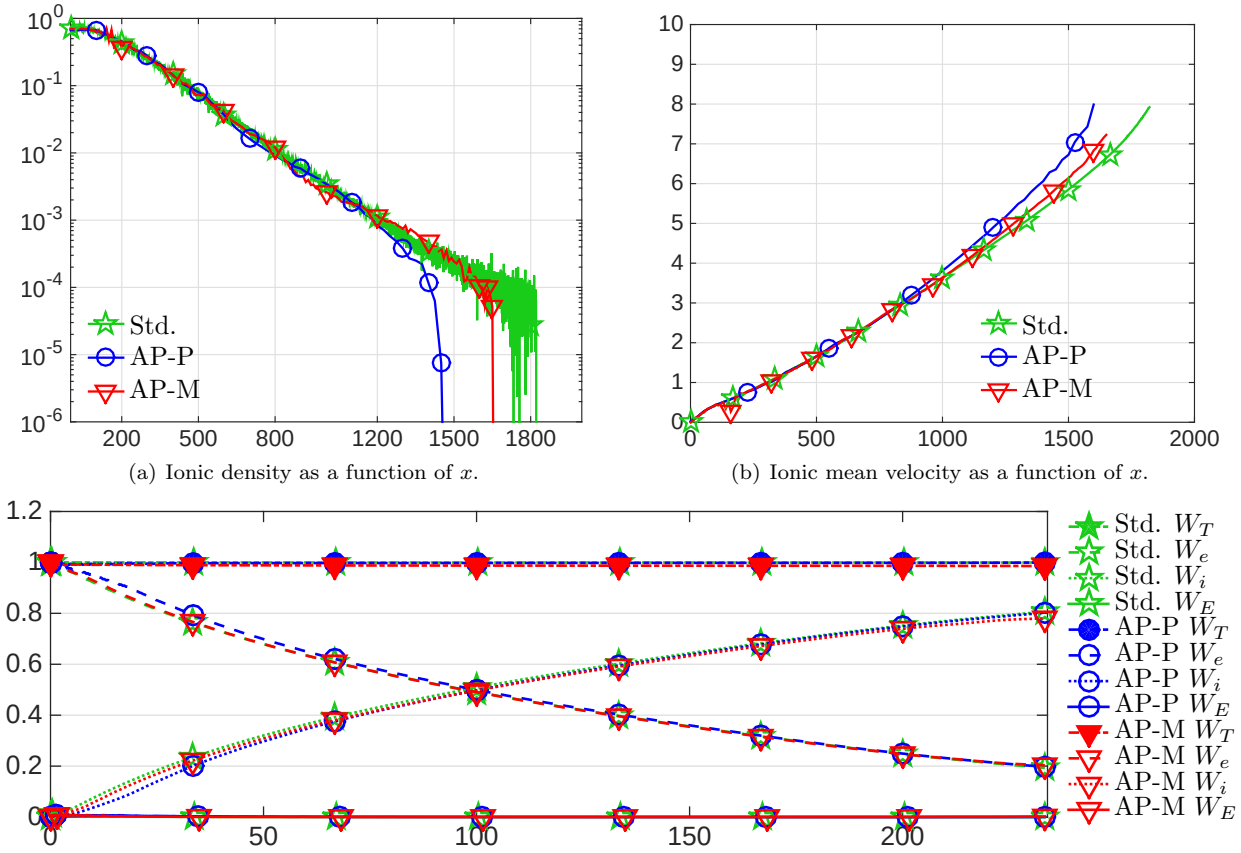

(a) Ionic density as a function of x.

(b) Ionic mean velocity as a function of x.

(c) Total (W_T), electronic (W_e), ionic (W_i) and electric (W_E) energies normalized by the initial electronic energy as functions of time.

Figure 3: Expansion of a high density plasma ($\lambda = \tau = 10^{-4}$): normalized ionic density ($n_i/n_{i,0}$) and mean velocity ($u_i/\sqrt{k_B T_{e,0}/m_i}$) as functions of the space variables x/λ_D at time $t = 233(\omega_{pi})$ computed thanks to a standard explicit scheme (Std.) with $\Delta x = 0.5\lambda_D$ and $\Delta t = 0.2\tau_p$ and 10^7 particles for each species, the AP-Particle scheme (AP-P) with $\Delta x = 25\lambda_D$ and $\Delta t = 5\tau_p$ and 10^6 particles and the AP-Moment (AP-M) with $\Delta x = 10\lambda_D$ and $\Delta t = 2\tau_p$ and 10^6 particles.

addressed thanks to a numerical method offering a transition from a MHD code into a PIC method [48]. The purpose here, is to demonstrate that the AP methods, based on an unified numerical scheme which can cope with both regimes, is an efficient alternative.

A 1D model of POS (already used in [21]) is first investigated, in order to compare the AP-schemes to a standard PIC method. Two dimensional simulations are then performed with a more complex physic, but without the modeling of the charge, so that, the operating of the device can not be simulated accurately up to the complete opening of the POS. Note also, that the field correction is not implemented for the two dimensional computations.

For sake of clarity, we state the equations of these two species model. The three-dimensional Cartesian coordinates are denoted by (x, y, z). The subscripts e and i indicate the species to which a field or a parameter is related. In the 1Dx-2Dv setting, the particles move along the x axis but have a velocity both in the x y directions. Thus, the electromagnetic field generated by the particles has only components E_x, E_y, and B_z.

Finally, the Vlasov-Maxwell model simplifies into the following equations:

$$\partial_t f_e + v_x \cdot \partial_x f_e + v_y \cdot \partial_y f_e - \frac{e}{m_e}(E_x + v_y B_z)\partial_{v_x} f_e - \frac{e}{m_e}(E_y - v_x B_z)\partial_{v_y} f_e = 0, \tag{104}$$

$$\partial_t f_i + v_x \cdot \partial_x f_i + v_y \cdot \partial_y f_i + \frac{e}{m_i}(E_x + v_y B_z)\partial_{v_x} f_i + \frac{e}{m_i}(E_y - v_x B_z)\partial_{v_y} f_i = 0, \tag{105}$$

$$\frac{1}{c^2}\partial_t E_x - \partial_y B_z = -\mu_0 J_x, \tag{106}$$

$$\frac{1}{c^2}\partial_t E_y + \partial_x B_z = -\mu_0 J_y, \tag{107}$$

$$\partial_t B_z + \partial_x E_y - \partial_y E_x = 0, \tag{108}$$

supplemented with the electric and magnetic Gauss laws.

The computational domain consists of the inter-electrode area with a length $L = 0.2$ (m). At the initial time, the plasma fills an area ranging in $x \in [0.05, 0.15]$. The plasma density is n_0 and the initial ion and electron velocities follow Maxwellian distributions with temperatures $T_i = T_e = 10^3$ eV. An electromagnetic wave (TEM mode) wave is sent on the plasma from the left side. The value of the ingoing electric field at the left end of the domain at time t is

$$E_{inc}(t) = A_{inc}\,(t/t_{inc})^{4/3}\left(8 + (t/t_{inc})^4\left((t/t_{inc})^8 - 6\right)\right), \tag{109}$$

where $A_{inc} = 1.8 \cdot 10^8$ V/m and $t_{inc} = 10^{-8}$ s. Transparent boundary conditions are prescribed at each end of the domain to avoid wave reflections.

5.4.2 A simplified 1D model of POS

A two specie plasma is simulated in a 1Dx-2Dv Vlasov-Maxwell model (one dimensional in space, two-dimensional in velocity). In the equations (104) - (108), this amounts to set $\partial_y f_e = \partial_y f_i = \partial_y B_z = \partial_y E_x = 0$.

The first investigations are related to low density configurations for which the computational cost required by a standard method remains workable. The main characteristics of the computations are presented in the table 1, all the computations being performed with $T_i = T_e = 10^3$ eV and $m_i/m_e = 2 \cdot 10^4$. The simulation results related to the set-up (Low-a) are displayed on the figure 4.

Set-up	Dens.	λ_D	ω_{pe}^{-1}	Std. scheme			AP schemes		
				$\Delta x\,(\bar{\lambda})$	$\Delta t\,(\bar{\tau})$	$\mathrm{N_p}$	$\Delta x\,(\bar{\lambda})$	$\Delta t\,(\bar{\tau})$	$\mathrm{N_p}$
(Low-a)	10^{16}	10^{-4}	10^{-10}	$10^{-4}\,(1)$	$10^{-11}(10)$	10^6	$10^{-4}\,(1)$	$10^{-11}(10)$	10^6
(Low-b)	10^{17}	$5\,10^{-5}$	$5\,10^{-11}$	$10^{-5}\,(5)$	$2\,10^{-12}(28)$	10^7	$10^{-3}\,(5\,10^{-2})$	$2\,10^{-12}(28)$	10^4
(High-a)	10^{20}	10^{-5}	10^{-11}				$10^{-3}\,(10^{-2})$	$10^{-11}(1)$	10^5
(High-b)	10^{22}	10^{-7}	10^{-13}				$10^{-3}\,(10^{-4})$	$10^{-11}(10^{-2})$	10^5

Table 1: Main characteristics of the computations related to the 1Dx-2Dv Plasma Opening Switch simulations: Plasma density (m^{-3}), initial Debye length (m) and plasma period (s), numerical parameters of the Standard (Std.) and the AP schemes: Mesh size (Δx) scaled Debye length ($\bar{\lambda} = \lambda/\Delta x$), time step ($\Delta t$) scaled plasma period $\bar{\tau} = \omega_{pe}^{-1}/\Delta t$ and total number of particles ($\mathrm{N_p}$).

The AP-schemes produce results comparable to the reference solution computed thanks to a standard scheme (defined by the equations (44-45), (48–52) and (57-58)) with a comparable level of numerical noise. The numerical methods give a good description of the electrostatic field existing in the sheath created at the plasma edge. In this region, the electrons, less massive than the ions, are the first expelled by the incident wave, breaking thus the quasi-neutrality of the plasma and creating a large electrostatic field (E_x component

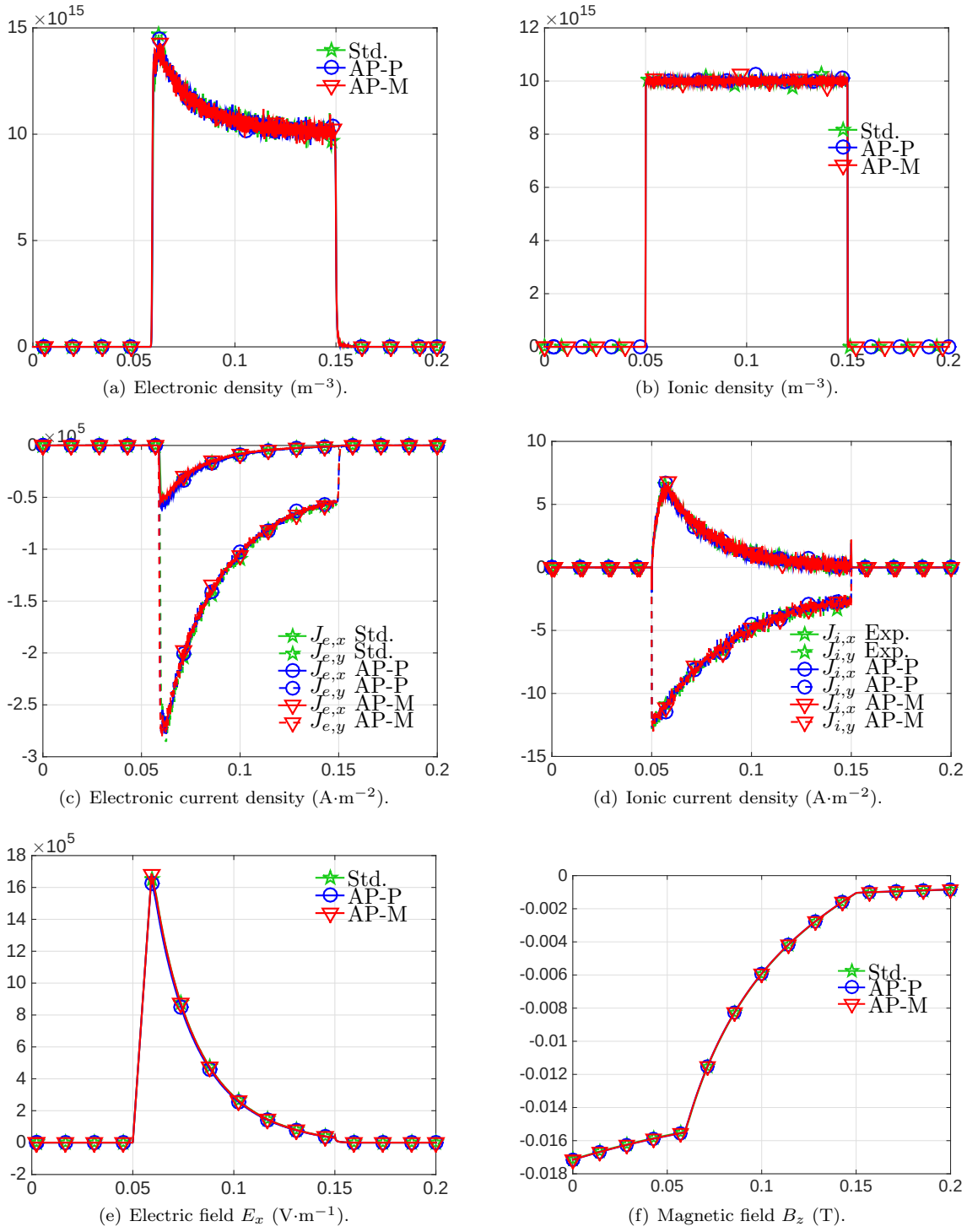

(a) Electronic density (m^{-3}).

(b) Ionic density (m^{-3}).

(c) Electronic current density ($\mathrm{A{\cdot}m}^{-2}$).

(d) Ionic current density ($\mathrm{A{\cdot}m}^{-2}$).

(e) Electric field E_x ($\mathrm{V{\cdot}m}^{-1}$).

(f) Magnetic field B_z (T).

Figure 4: Low density POS (Set-up Low-a detailed in table 1): Particle density, electronic and ionic current components in the x (plain line) and y (dashed line) directions and electromagnetic field as functions of the space variable x at time $t = 3 \cdot 10^{-9}$s as computed by a standard numerical method (Std.), the AP-moment (AP-M) and AP-particle (AP-P) schemes.

of the electric field). This electrostatic field gradually accelerates the ions. This process cannot be well accounted for without a good consistency of the numerical method with the Gauss-law, the simulations performed without the field correction produce indeed electrons separating from the ions without an electric field response to restore the system quasi-neutrality. For the lowest plasma densities, the magnetic field is observed to be significantly transmitted trough the plasma. However, with the density increase, the currents created by the electron motion at the plasma edge are strong enough to slow down the penetration of the magnetic field into the plasma bulk as depicted on the figure 5 related to the set-up (low-b) ran with a density ten times larger. Note that the computations performed thanks to the AP-schemes used a mesh size two order of magnitude larger than the Debye length and than the mesh size used for the standard method. Even though the mesh resolution used for the AP-schemes is coarser than the one of the standard method, all the numerical results are totally indistinguishable. For the highest plasma densities, the magnetic field is almost entirely reflected at the plasma edge due to the large current generated by the electron flow. This can be observed on the figure 6 related to plasma densities as large as $10^{20} - 10^{22}$ m^{-3}. For these values, the standard methods exhibit a prohibitive computational cost so that no reference solution can be carried out for these set-up. The computations are possible with the AP methods thanks to the large value of the mesh size used compared to the Debye length. For the most demanding computations, this represents a gain of four order of magnitude in the number of cells and consequently in the number of numerical particles. Significant gain are also obtained thanks to the use of a time step large compared to the plasma period (see table 1).

5.4.3 Two dimensional simulations of Plasma Opening Switches

This two dimensional simulation is devoted to the propagation of the magnetic field into the plasma bulk by means of a shock wave [49] also referred to as a KMC wave (for Kingsep, Mokhov and Chukbar [35]). This non linear phenomenon is exhibited from the equations in the quasi neutral limit, it constitutes thus a perfect means of demonstrating the consistency of the AP-method with the quasi-neutral regime. Considering the Ohm's law, consisting of the electronic momentum equation with inertia and pressure terms neglected, the following definition of the electric field holds

$$E + \big(u - J/(en)\big) \times B = 0$$

where u is the mean velocity of the ions assumed to be at rest (u=0) and thanks to the Ampere's equation, $\nabla \times B = \mu_0 J$, we obtain

$$\partial_t B = -\nabla \times \big((\nabla \times B \times B)/(\mu_0 en)\big)\,,$$

so that, the magnetic evolution is governed by the only Hall term. In the spatial framework investigated so far, the bi-dimensional computational domain is immersed in the (x, y)-plane with a magnetic field being reduced to the B_z component, all the quantities only depending on the space variables x and y and on time. Neglecting the variation of the density along the x coordinate yields to a simplified model for the evolution of the magnetic field which writes

$$\partial_t B_z = -\frac{1}{e2\mu_0}\partial_y\left(\frac{1}{n}\right)\partial_x B_z^2\,.$$

This shows that the magnetic field can penetrate the plasma, when a transverse gradient exists, with a velocity estimated by

$$V_{\mathrm{KMC}} = \frac{B_z}{e\mu_e}\partial_y\frac{1}{n}\,. \tag{110}$$

This furnishes a good means of verification for the AP-methods in the quasi-neutral limit. In this aim, two simulations have been performed, on a coarse mesh with few particles and a second one with a more refined mesh as well as an increased number of particles. The electrons is the only specie advanced, the ions remaining motionless. The main parameters defining the test cases are gathered in figure 8. The evolution of the magnetic field can be observed on figure 7 demonstrating a rapid magnetization of the plasma in the region where the initial density gradient is located. The electrons emitted at the cathode produce a current

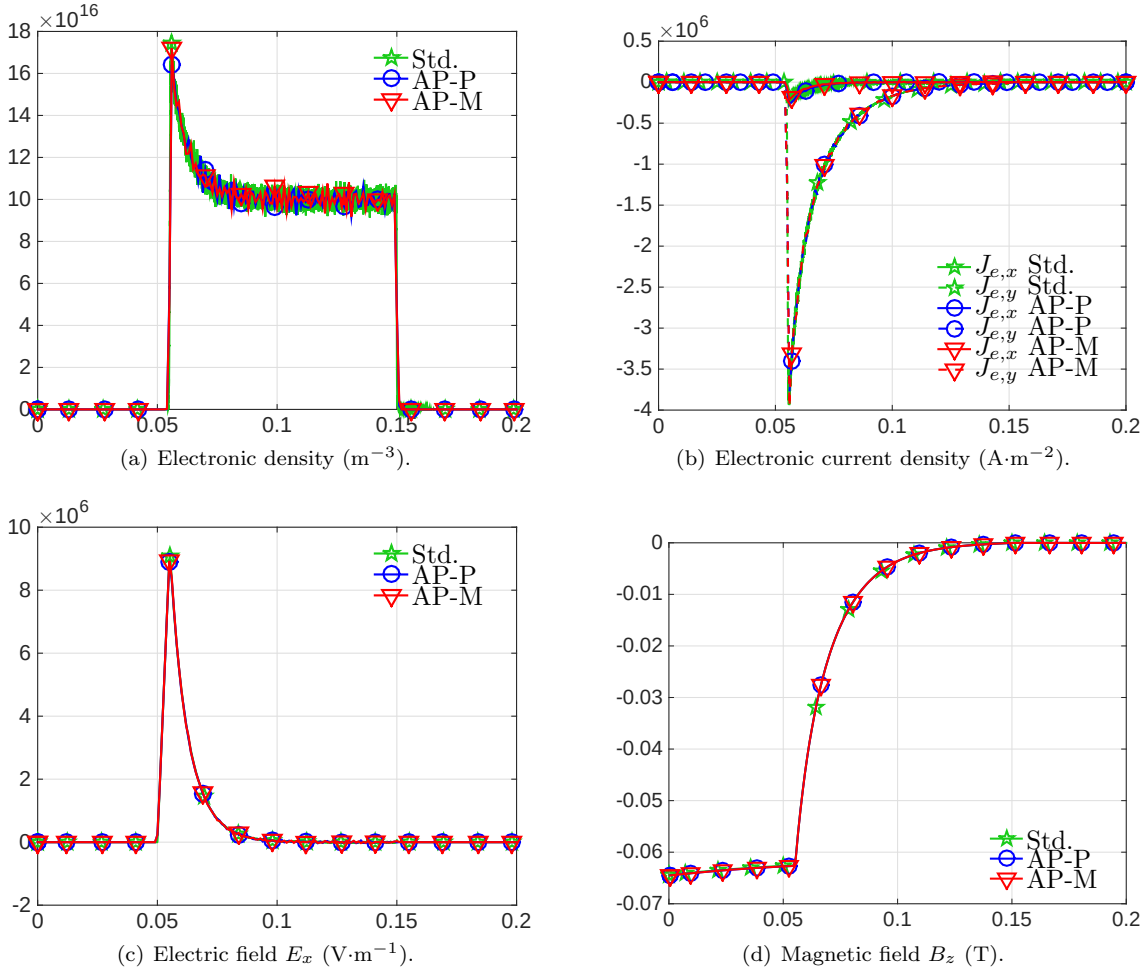

(a) Electronic density (m^{-3}).

(b) Electronic current density ($\mathrm{A}\cdot\mathrm{m}^{-2}$).

(c) Electric field E_x ($\mathrm{V}\cdot\mathrm{m}^{-1}$).

(d) Magnetic field B_z (T).

Figure 5: Low density POS (Set-up Low-b detailed in table 1): Electronic particle density and current in the x (plain line) and y (dashed line) directions and electromagnetic field as functions of the space variables x at time $t = 4 \cdot 10^{-9}$s as computed by a standard numerical method (Std.), the AP-moment (AP-M) and AP-particle (AP-P) schemes.

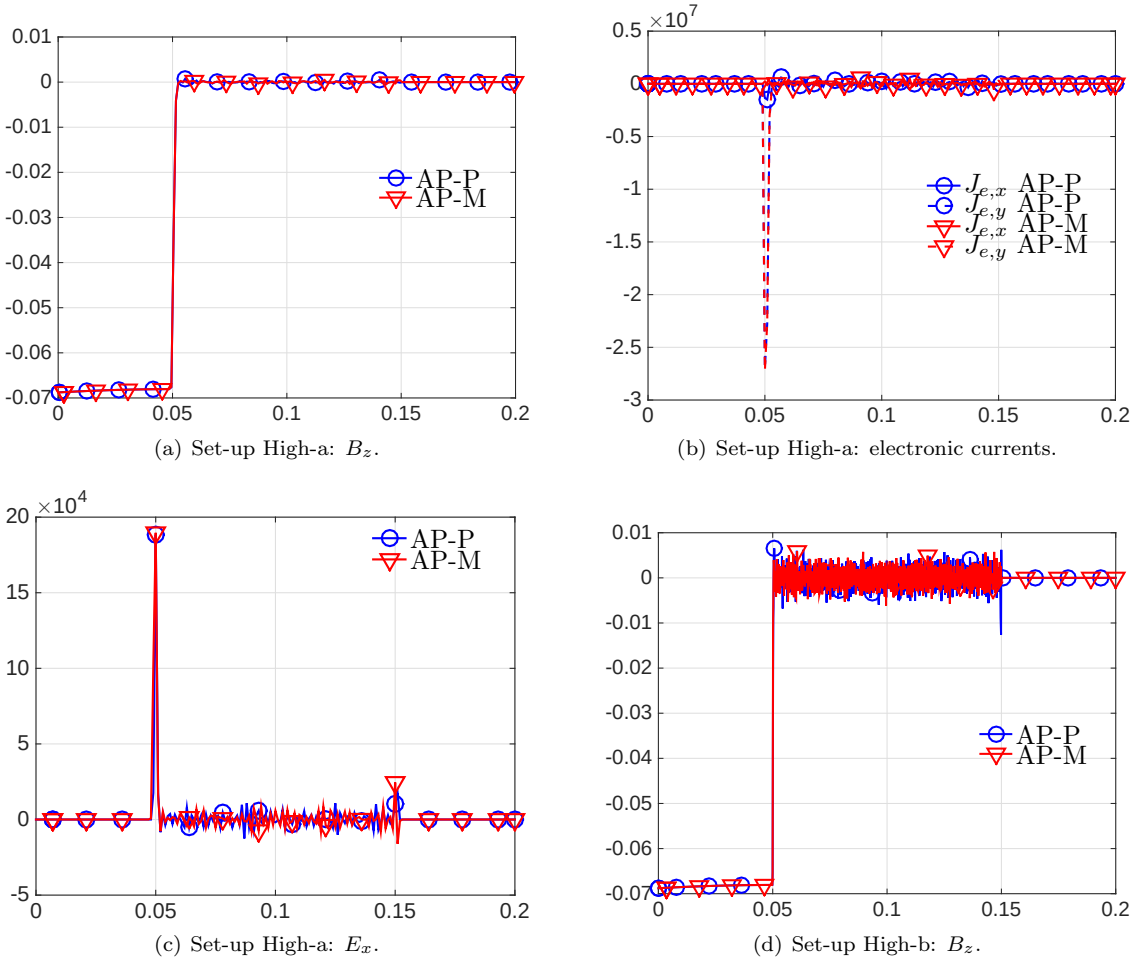

(a) Set-up High-a: B_z.

(b) Set-up High-a: electronic currents.

(c) Set-up High-a: E_x.

(d) Set-up High-b: B_z.

Figure 6: High density POS (Set-up High-a and High-b of table 1) : Magnetic field B_z (T), electronic currents (A·m^{-2}) and electrostatic field (V/m) as a functions of the space variable x at time $t = 4 \cdot 10^{-9}$s as computed by the AP-moment (AP-M) and AP-particle (AP-P) schemes

which prevents a uniform penetration of the magnetic field in the plasma. This current is gradually deflected with the propagation of the magnetic field, as depicted on figures 7(c) and 7(d). The propagation speed of the magnetic field is evaluated thanks to the successive positions of the extremity of the field magnitude level set at different simulated times. The data related to the level set are displayed on figures 8(a) and 8(b) and the estimated velocities as well as the reference value computed thanks to the relation (110) are compared in the tabular included in the figure 8. A very good agreement is obtained with the set-up (a), the KMC speed mean value estimated thanks to the simulations being 76% that of the theoretical expression, with a significant improvement on the refined mesh (set-up (b)), the estimation reaching 82% of the theoretical value. Important also is the value of the Debye length characterizing these simulations and more specifically its scaling with respect to the mesh sizes. In the most demanding case, the mesh size is roughly four order of magnitudes larger than the Debye length. However, the macroscopic evolution of all the quantities is well reproduced which of course improves significantly the efficiency of the AP-method as compared to standard explicit schemes.

6 Conclusion

In this paper, we have introduced a quasi-neutral limit of the Vlasov-Maxwell system and derived Asymptotic-Preserving Particle-In-Cell methods able to account accurately for quasi-neutral as well as non quasi-neutral phenomena. The main advantage of these methods is their ability to offer a consistancy with either the quasi-neutral model or the standard (non quasi-neutral) system accordingly to how the discretization parameters resolve the plasma parameters. No rigorous numerical analysis is provided in this paper, and this should be the subject of future work. However, the numerous numerical investigations performed in the electrostatic as well as the electromagnetic frameworks, demonstrate conclusively the efficiency of the introduced schemes, to account for phenomenon evolving on the plasma period and Debye length, as well as phenomenon well accounted for by the MHD theory, with the ability to cope with vacuum to dense interfaces and the formation of non neutral sheaths. Although some implicit Particle-In-Cell methods may share analogous properties, the methodology developed in this paper, based on the reformulation of the equations, represents a breakthrough as compared to the existing approaches, namely implicit or semi implicit discretization of PIC methods. The systematic derivation securing the Asymptotic-Preserving property, as developed in this paper, is for us the main achievement of the present work, that opens the way for addressing more singular asymptotic limits and derive numerical method with an improved efficiency.

Acknowledgments. This work has been carried out within the framework of the EUROfusion Consortium and has received funding from the Euratom research and training programme 2014-2018 under grant agreement No 633053. The views and opinions expressed herein do not necessarily reflect those of the European Commission.
Furthermore, the authors would like to acknowledge support from the ANR PEPPSI (Plasma Edge Physics and Plasma-Surface Interactions, 2013-2017) and ANR MOONRISE (MOdels, Oscillations and NumeRIcal SchEmes, 2014-2018).

A Properties of the θ-scheme for the Maxwell equations

Consider the Maxwell equations in $\mathbb{R}^d$, discretized with a Yee lattice in space and a θ-scheme in time:

$$\frac{1}{c^2}\frac{E_h^{m+1}-E_h^m}{\Delta t} - \nabla_h \times \bar{B}_h^{m+\theta} = -\mu_0 J_h^{m+1}, \tag{111}$$

$$\frac{B_h^{m+1}-B_h^m}{\Delta t} + \nabla_h \times \bar{E}_h^{m+\theta} = 0. \tag{112}$$

The following proposition recalls some results on the stability, the energy balance and the dispersion properties of the above discretization.

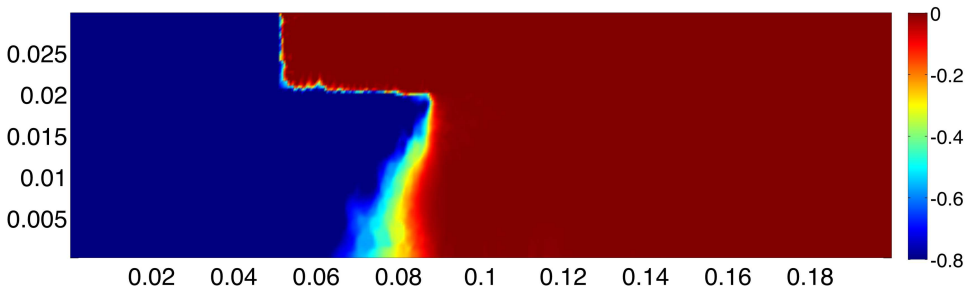

(a) Magnetic field B_z at time t_4.

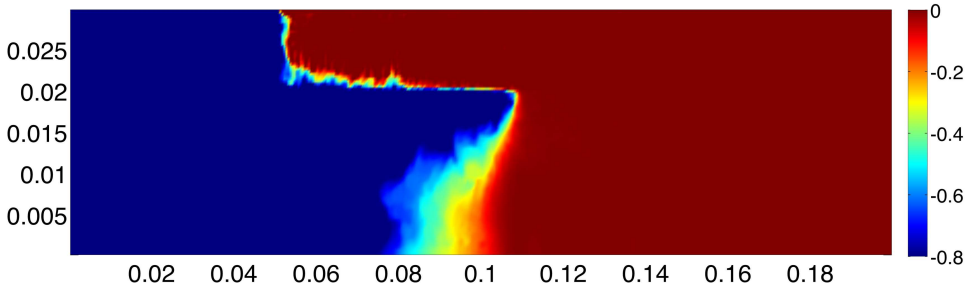

(b) Magnetic field B_z at time t_6.

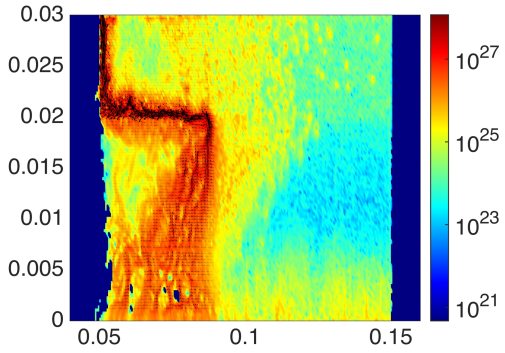

(c) Current density J_e at time t_4.

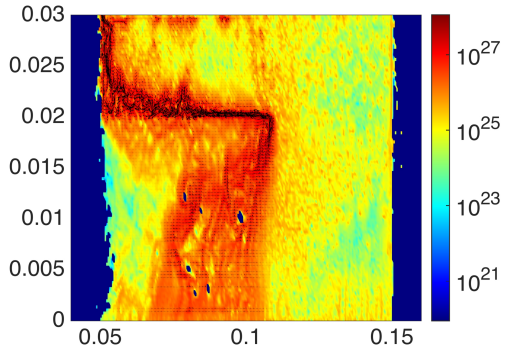

(d) Current density J_e at time t_6.

Figure 7: KMC wave propagation: magnetic field (B_z in Tesla) and electronic current density (J_e in A$\cdot$ m^{-2} in decimal log-scale, the colour scale being related to the power of ten) as functions of the space coordinates at time $t_4 = 2.58$ns and $t_6 = 3.67$ns computed with the set-up (b) detailed in figure 8.

Proposition A.1. *(i) The following energy balance holds true:*

$$\mathcal{E}_h^{m+1} - \mathcal{E}_h^m = -\left(\theta - \frac{1}{2}\right)\left(\epsilon_0 \left(E_h^{m+1} - E_h^m\right)^2 + \frac{1}{\mu_0}\left(B_h^{m+1} - B_h^m\right)^2\right) - \Delta t J_h^{m+1} \cdot \bar{E}_h^{m+\theta}, \tag{113}$$

where $\mathcal{E}_h^m := \frac{\epsilon_0}{2}\|E_h^m\|^2 + \frac{1}{2\mu_0}\|B_h^m\|^2$. *In particular, for* $\theta = \frac{1}{2}$,

$$\mathcal{E}_h^{m+1} - \mathcal{E}_h^m = -\Delta t J_h^{m+1} \cdot \bar{E}_h^{m+\theta}. \tag{114}$$

(ii) Therefore, the scheme is unconditionally stable for $\theta \in [\frac{1}{2}, 1]$.
(iii) In 1D, for $\theta = \frac{1}{2}$, *the ratio between the phase velocity of a discrete wave plane and the continuous wave*

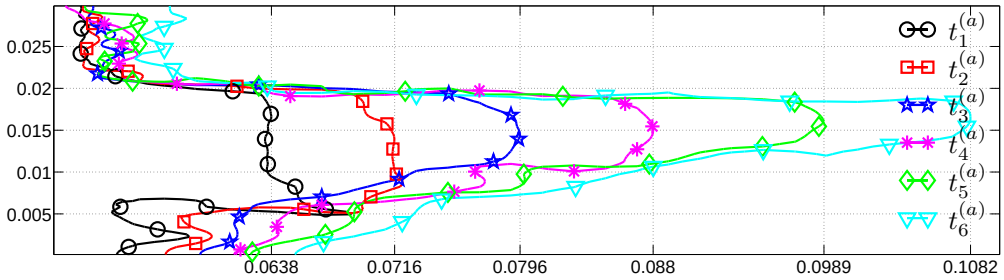

(a) Magnetic field level set as a function of the x and y space variables at times $t_1^{(a)} = 1.75$, $t_2^{(a)} = 2.16$, $t_3^{(a)} = 2.56$, $t_4^{(a)} = 3.03$, $t_5^{(a)} = 3.56$ and $t_6^{(a)} = 4.09$ ns (set-up (a)).

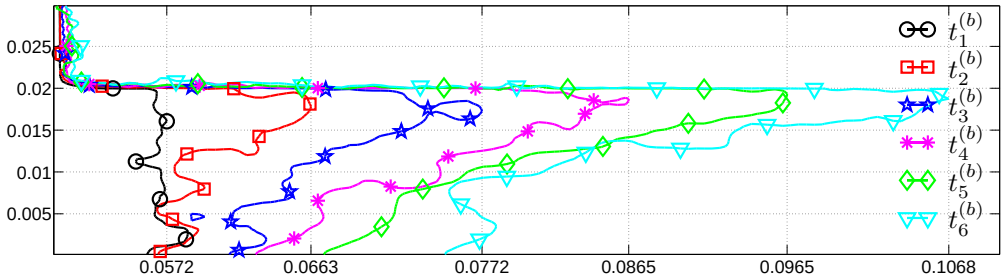

(b) Magnetic field level set as a function of the x and y space variables at times $t_1^{(b)} = 1.24$, $t_2^{(b)} = 1.62$, $t_3^{(b)} = 2.06$, $t_4^{(b)} = 2.58$, $t_5^{(b)} = 3.11$ and $t_6^{(b)} = 3.67$ ns (set-up (b)).

Set-up	Density	T_e	$\bar{\lambda}$	V_{KMC}	V_{1-2}	V_{2-3}	V_{3-4}	V_{4-5}	V_{5-6}
	m^{-3}	K		$\times 10^6\ \text{m}\cdot\text{s}^{-1}$					
(a)	$10^{19} - 10^{20}$	$6\ 10^4$	$8.3\,10^{-4} - 5.5\,10^{-3}$	25	19.4	19.8	17.8	20.7	17.3
(b)	$10^{19} - 10^{21}$	$6\ 10^2$	$1.1\,10^{-4} - 1.8\,10^{-4}$	25	24.3	24.8	17.9	18.8	18.2

Figure 8: KMC wave velocity (V_{KMC}) as computed by equation (110) and estimated (V_{i-j}) thanks to the evolution of the magnetic field level set ($B_z = -0.8$ Tesla) on the time interval $[t_i, t_j]$. The simulations are performed with two sets of parameters: Set-up (a) (resp. (b)) relates to a grid with 100×100 (resp. 400×100) cells and 10^5 (resp. $4\ 10^6$) particles. The density gradient in the plasma bulk is located in the range $y \in [0.01,\ 0.02]$ for both set-ups (the extrema values are defined in column 2), the electron temperature being precised in column 3. The parameter $\bar{\lambda}$ is defined as the ratio of the Debye length and the mesh size in the x and y directions.

plane of wavenumber k is

$$\frac{\omega_d}{\omega} = \pm \frac{2}{kh} \frac{h}{c\Delta t} \arctan\left(\frac{c\Delta t}{h} \sin\left(\frac{kh}{2} \right) \right). \tag{115}$$

Dispersion curves of the Crank-Nicolson scheme in 1D for different values of the Courant number are represented in the figure below. We note that, even with a Courant number equal to 1, the Crank-Nicolson scheme is dispersive, unlike the leap-frog scheme.

B Particle pusher

The time-integration scheme for advancing the particles within the AP numerical method is investigated in this section and more precisely on the discretization of the electric force. Let us consider the following

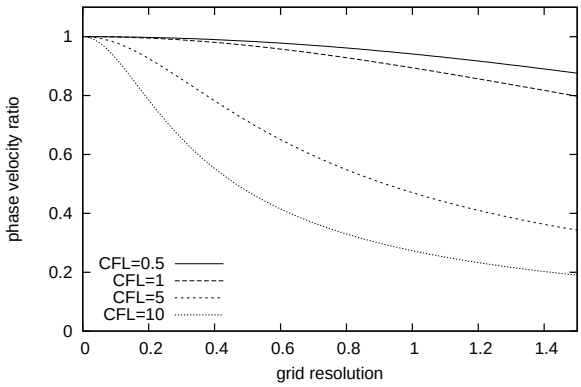

Figure 9: Dispersion of the Crank-Nicolson scheme for different values of the Courant number.

Euler-like schemes:

$$\frac{X_{N,j}^{m+1} - X_{N,j}^{m}}{\Delta t} = V_{N,j}^{m+b}, \qquad \forall j \in \{1, \dots, N\}, \tag{116}$$

$$\frac{V_{N,j}^{m+1} - V_{N,j}^{m}}{\Delta t} = -E_h^{m+c}(X_{N,j}^{m+a}), \qquad \forall j \in \{1, \dots, N\}, \tag{117}$$

where $(a, b, c) \in \{0, 1\}^3$. The numerical simulations we have performed show that the electric field and the velocity must be made implicit ($b = 1$, $c = 1$) to overcome the stability condition (53). They also show that, whatever the choice for (a, b, c), the scheme remains subject to the Courant condition (55). An explicit discretization of the position ($a = 0$) is preferable to an implicit discretization ($a = 1$), since it yields a scheme with better conservation properties (see Remark B.1 below) and easier to solve.

Remark B.1. *Let us consider the motion of a particle in a constant electric field E_0. The position $X(t)$ and the velocity $V(t)$ of the particle satisfy the system of ordinary differential equations:*

$$\partial_t X(t) = V(t), \tag{118}$$

$$\partial_t V(t) = -E_0(X(t)). \tag{119}$$

It is well-known that this system is Hamiltonian. For such a system, it is recommended to use symplectic time-integration schemes. They ensure good conservation properties and an accurate behavior in long-time simulations [28]. Euler schemes for solving this system are:

$$\frac{X^{m+1} - X^{m}}{\Delta t} = V^{m+a}, \tag{120}$$

$$\frac{V_{N,j}^{m+1} - V_{N,j}^{m}}{\Delta t} = -E_0(X^{m+b}), \tag{121}$$

where $(a, b) \in \{0, 1\}^2$. The semi-implicit Euler schemes (corresponding to parameters $a = 1$ and $b = 0$, or $a = 0$ and $b = 1$) are symplectic, unlike the fully implicit Euler scheme ($a = 1$ and $b = 1$).

References

[1] M. Acheritogaray, P. Degond, A. Frouvelle, and J.-G. Liu. Kinetic formulation and global existence for the hall-magneto-hydrodynamics system. *Kinetic and Related Models*, 4(4):901–918, Nov. 2011.

[2] J. C. Adam, A. Gourdin Serveniere, J.-C. Nédélec, and P.-A. Raviart. Study of an implicit scheme for integrating Maxwell's equations. *Comput. Methods Appl. Mech. Engrg.*, 22(3):327–346, 1980.

[3] R. Barthelmé. *Le problème de de conservation de la charge dans le couplage des équations de Vlasov et de Maxwell.* PhD thesis, Université de Strasbourg, 2005.

[4] R. Barthelmé, P. Ciarlet, Jr., and E. Sonnendrücker. Generalized formulations of Maxwell's equations for numerical Vlasov-Maxwell simulations. *Math. Models Methods Appl. Sci.*, 17(5):657–680, 2007.

[5] R. Belaouar, N. Crouseilles, P. Degond, and E. Sonnendrücker. An asymptotically stable semi-Lagrangian scheme in the quasi-neutral limit. *J. Sci. Comput.*, 41(3):341–365, 2009.

[6] C. Birdsall and A. Langdon. *Plasma physics via computer simulation.* Inst of Physics Pub Inc, 2004.

[7] J. Boris. Relativistic plasma simulation-optimization of a hybrid code. In *Proceedings*, page 3. Naval Research Laboratory; for sale by the Supt. of Docs., US Govt. Print Off., 1972.

[8] K. Bowers. Implicit methods of solving the Maxwell equations suitable for particle-in-cell simulation of low temperature plasmas. *preprint*, 2001.

[9] J. U. Brackbill and D. W. Forslund. An implicit method for electromagnetic plasma simulation in two dimensions. *J. Comput. Phys.*, 46(2):271–308, 1982.

[10] A. Catella, V. Dolean, and S. Lanteri. An unconditionally stable discontinuous galerkin method for solving the 2-d time-domain maxwell equations on unstructured triangular meshes. *Magnetics, IEEE Transactions on*, 44(6):1250–1253, 2008.

[11] F. Chen. *Introduction to plasma physics and controlled fusion: Plasma physics.* Plenum Pub Corp, 1984.

[12] G. Chen, L. Chacón, and D. C. Barnes. An energy- and charge-conserving, implicit, electrostatic particle-in-cell algorithm. *Journal of Computational Physics*, 230(18):7018–7036, Aug. 2011.

[13] G. Chen, L. Chacón, and D. C. Barnes. An efficient mixed-precision, hybrid CPUGPU implementation of a nonlinearly implicit one-dimensional particle-in-cell algorithm. *Journal of Computational Physics*, 231(16):5374–5388, June 2012.

[14] G. Chen, L. Chacón, C. A. Leibs, D. A. Knoll, and W. Taitano. Fluid preconditioning for newtonkrylov-based, fully implicit, electrostatic particle-in-cell simulations. *Journal of Computational Physics*, 258:555–567, Feb. 2014.

[15] B. I. Cohen, A. Langdon, D. W. Hewett, and R. J. Procassini. Performance and optimization of direct implicit particle simulation. *Journal of Computational Physics*, 81(1):151 – 168, 1989.

[16] B. L. Cohen, A. B. Langdon, and A. Friedman. Implicit time integration for plasma simulation. *J. Comput. Phys.*, 46(1):15–38, 1982.

[17] P. Crispel, P. Degond, and M.-H. Vignal. An asymptotic preserving scheme for the two-fluid Euler-Poisson model in the quasineutral limit. *J. Comput. Phys.*, 223(1):208–234, 2007.

[18] N. Crouseilles, T. Respaud, and E. Sonnendrcker. A forward semi-lagrangian method for the numerical solution of the vlasov equation. *Computer Physics Communications*, 180(10):1730 – 1745, 2009.

[19] P. Degond. Asymptotic-preserving schemes for fluid models of plasmas. *arXiv:1104.1869*, 39-40:1–90, 2013.

[20] P. Degond, F. Deluzet, L. Navoret, A.-B. Sun, and M.-H. Vignal. Asymptotic-preserving particle-in-cell method for the Vlasov-Poisson system near quasineutrality. *J. Comput. Phys.*, 229(16):5630–5652, 2010.

[21] P. Degond, F. Deluzet, and D. Savelief. Numerical approximation of the Euler-Maxwell model in the quasineutral limit. *Journal of Computational Physics*, 231(4):1917 – 1946, 2012.

[22] F. Deluzet. Mathematical modeling of plasma opening switches. *Comput. Phys. Commun.*, 152(1):34–54, 2003.

[23] M. Drouin, L. Gremillet, J.-C. Adam, and A. Hron. Particle-in-cell modeling of relativistic laserplasma interaction with the adjustable-damping, direct implicit method. *Journal of Computational Physics*, 229(12):4781 – 4812, 2010.

[24] R. Fernsler, S. Slinker, and G. Joyce. Quasineutral plasma models. *Physical Review E*, 71(2), Feb. 2005.

[25] A. Fruchtman, J. Grossmann, S. Swanekamp, and P. Ottinger. Sheath propagation along the cathode of a plasma opening switch. *IEEE Transactions on Plasma Science*, 27(5):1464–1468, Oct. 1999.

[26] M. R. Gibbons and D. W. Hewett. The darwin direct implicit particle-in-cell (DADIPIC) method for simulation of low frequency plasma phenomena. *Journal of Computational Physics*, 120(2):231–247, Sept. 1995.

[27] T. Grismayer, P. Mora, J. Adam, and A. Héron. Electron kinetic effects in plasma expansion and ion acceleration. *Physical Review E*, 77(6):066407, 2008.

[28] E. Hairer, C. Lubich, and G. Wanner. *Geometric numerical integration*, volume 31 of *Springer Series in Computational Mathematics*. Springer-Verlag, Berlin, 2002. Structure-preserving algorithms for ordinary differential equations.

[29] D. Han Kwan. *Contribution à l'étude mathématique des plasmas fortement magnétisés*. PhD thesis, Université Paris VI, 2011.

[30] D. W. Hewett. Low-frequency electromagnetic (Darwin) applications in plasma simulation. *Computer Physics Communications*, 84(13):243–277, Nov. 1994.

[31] D. W. Hewett and A. B. Langdon. Electromagnetic direct implicit plasma simulation. *Journal of Computational Physics*, 72(1):121 – 155, 1987.

[32] R. Hockney and J. Eastwood. *Computer simulation using particles*. Taylor & Francis, 1988.

[33] S. Jin. Efficient asymptotic-preserving (AP) schemes for some multiscale kinetic equations. *SIAM J. Sci. Comput.*, 21(2):441–454, 1999.

[34] G. Joyce, M. Lampe, S. P. Slinker, and W. M. Manheimer. Electrostatic particle-in-cell simulation technique for quasineutral plasma. *Journal of Computational Physics*, 138(2):540–562, 1997.

[35] A. S. Kingsep, Y. V. Mokhov, and K. V. Chukbar. Nonlinear skin phenomena in plasma. In *Nonlinear and Turbulent Processes in Physics*, volume -1, page 267, 1984.

[36] A. B. Langdon. On enforcing gauss' law in electromagnetic particle-in-cell codes. *Computer Physics Communications*, 70(3):447 – 450, 1992.

[37] A. B. Langdon, B. I. Cohen, and A. Friedman. Direct implicit large time-step particle simulation of plasmas. *J. Comput. Phys.*, 51(1):107–138, 1983.

[38] I. Langmuir. The interaction of electron and positive ion space charges in cathode sheaths. *Physical Review*, 33(6):954–989, 1929.

[39] G. Lapenta. Particle simulations of space weather. *Journal of Computational Physics*, 231(3):795–821, Feb. 2012.

[40] G. Lapenta, J. U. Brackbill, and P. Ricci. Kinetic approach to microscopic-macroscopic coupling in space and laboratory plasmasa). *Physics of Plasmas (1994-present)*, 13(5):055904, May 2006.

[41] G. Manfredi, S. Hirstoaga, and S. Devaux. Vlasov modelling of parallel transport in a tokamak scrape-off layer. *Plasma Physics and Controlled Fusion*, 53(1):015012, Jan. 2011.

[42] S. Markidis and G. Lapenta. The energy conserving particle-in-cell method. *Journal of Computational Physics*, 230(18):7037–7052, Aug. 2011.

[43] S. Markidis, G. Lapenta, and Rizwan-uddin. Multi-scale simulations of plasma with iPIC3d. *Mathematics and Computers in Simulation*, 80(7):1509–1519, Mar. 2010.

[44] R. J. Mason. Implicit moment particle simulation of plasmas. *J. Comput. Phys.*, 41(2):233–244, 1981.

[45] R. J. Mason. An electromagnetic field algorithm for 2D implicit plasma simulation. *J. Comput. Phys.*, 71(2):429–473, 1987.

[46] P. Ricci, G. Lapenta, and J. U. Brackbill. A simplified implicit Maxwell solver. *J. Comput. Phys.*, 183(1):117–141, 2002.

[47] A. Richardson, D. Hinshelwood, P. Ottinger, J. Schumer, S. Swanekamp, and T. Mehlhorn. Particle-in-cell simulations of species separation in the plasma opening switch. In *2012 Abstracts IEEE International Conference on Plasma Science (ICOPS)*, pages 1P–99–1P–99, July 2012.

[48] J. Schumer, S. Swanekamp, P. Ottinger, R. Commisso, B. Weber, D. N. Smithe, and L. Ludeking. MHD-to-PIC transition for modeling of conduction and opening in a plasma opening switch. *IEEE Transactions on Plasma Science*, 29(3):479–493, June 2001.

[49] S. B. Swanekamp, J. M. Grossmann, A. Fruchtman, B. V. Oliver, and P. F. Ottinger. Particleincell simulations of fast magnetic field penetration into plasmas due to the hall electric field. *Physics of Plasmas (1994-present)*, 3(10):3556–3563, Oct. 1996.

[50] A. Taflove, S. Hagness, et al. *Computational electrodynamics: The finite-difference time-domain method*. Artech House Norwood, MA, 2000.

[51] W. Taitano, D. Knoll, L. Chacón, and G. Chen. Development of a consistent and stable fully implicit moment method for vlasov–ampre particle in cell (PIC) system. *SIAM Journal on Scientific Computing*, 35(5):S126–S149, Jan. 2013.

[52] H. Vu and J. Brackbill. Celest1d: an implicit, fully kinetic model for low-frequency, electromagnetic plasma simulation. *Computer physics communications*, 69(2-3):253–276, 1992.

[53] J. M. Wallace, J. U. Brackbill, and D. W. Forslund. An implicit moment electromagnetic plasma simulation in cylindrical coordinates. *Journal of Computational Physics*, 63(2):434 – 457, 1986.

[54] Z. Zeng, Y. Qiu, and E. Kuffel. A particle-in-cell simulation of plasma opening switch. In L. G. Christophorou and J. K. Olthoff, editors, *Gaseous Dielectrics IX*, pages 155–160. Springer US, Jan. 2001.